NAVAL POSTGRADUATE SCHOOL

MONTEREY, CALIFORNIA

THESIS

RADAR ENVELOPE VISUALIZATION

by

David A. Tan

June 2018

Thesis Advisor: Loren E. Peitso
Second Reader: Donald P. Brutzman

Approved for public release. Distribution is unlimited.

THIS PAGE INTENTIONALLY LEFT BLANK

REPORT DOCUMENTATION PAGE			*Form Approved OMB No. 0704-0188*

1. AGENCY USE ONLY *(Leave blank)*	**2. REPORT DATE** June 2018	**3. REPORT TYPE AND DATES COVERED** Master's thesis

4. TITLE AND SUBTITLE RADAR ENVELOPE VISUALIZATION	**5. FUNDING NUMBERS**
6. AUTHOR(S) David A. Tan	
7. PERFORMING ORGANIZATION NAME(S) AND ADDRESS(ES) Naval Postgraduate School Monterey, CA 93943-5000	**8. PERFORMING ORGANIZATION REPORT NUMBER**
9. SPONSORING / MONITORING AGENCY NAME(S) AND ADDRESS(ES) N/A	**10. SPONSORING / MONITORING AGENCY REPORT NUMBER**

11. SUPPLEMENTARY NOTES The views expressed in this thesis are those of the author and do not reflect the official policy or position of the Department of Defense or the U.S. Government.

12a. DISTRIBUTION / AVAILABILITY STATEMENT Approved for public release. Distribution is unlimited.	**12b. DISTRIBUTION CODE** A

13. ABSTRACT (maximum 200 words)

The Navy and Marine Corps cannot expect to always operate aircraft within permissive environments. Potential employment scenarios include operations against advanced surface-to-air missiles and early warning radars with detection ranges advertised beyond 200 nautical miles. Low-observable aircraft are not a panacea. Very-low frequency radars and multistatic arrays offer limited direction finding and possible ranging of fifth-generation aircraft at tactically significant ranges in certain conditions. Radar directed weapons will continue to be the most capable and deadly weapons aviation must contend with for the foreseeable future.

This project provides a proof-of-concept for a program that generates a three-dimensional volume representative of threat radar performance, which will aid planners in developing routes that avoid or minimize exposure to these threats and improve understanding of other radar phenomena. This representation includes a basic atmosphere model that demonstrates the effects of refraction, a depiction of the shadow zone, and terrain-masking effects. Future development would allow inclusion of location-specific weather and simulation of specific threat radars, allowing near real-time evaluation of radar capabilities that greatly exceed the abilities of current analytical tools.

14. SUBJECT TERMS RADAR, visualization, MOVES, simulation, horizon, X3D, extensible, 3D, graphics	**15. NUMBER OF PAGES** 83
	16. PRICE CODE

17. SECURITY CLASSIFICATION OF REPORT	**18. SECURITY CLASSIFICATION OF THIS PAGE**	**19. SECURITY CLASSIFICATION OF ABSTRACT**	**20. LIMITATION OF ABSTRACT**
Unclassified	Unclassified	Unclassified	UU

NSN 7540-01-280-5500 Standard Form 298 (Rev. 2-89) Prescribed by ANSI Std. 239-18

THIS PAGE INTENTIONALLY LEFT BLANK

Approved for public release. Distribution is unlimited.

RADAR ENVELOPE VISUALIZATION

David A. Tan
Captain, United States Marine Corps
BS, U.S. Naval Academy, 2012

Submitted in partial fulfillment of the
requirements for the degree of

MASTER OF SCIENCE IN COMPUTER SCIENCE

from the

NAVAL POSTGRADUATE SCHOOL
June 2018

Approved by: Loren E. Peitso
Advisor

Donald P. Brutzman
Second Reader

Peter J. Denning
Chair, Department of Computer Science

THIS PAGE INTENTIONALLY LEFT BLANK

ABSTRACT

The Navy and Marine Corps cannot expect to always operate aircraft within permissive environments. Potential employment scenarios include operations against advanced surface-to-air missiles and early warning radars with detection ranges advertised beyond 200 nautical miles. Low-observable aircraft are not a panacea. Very-low frequency radars and multistatic arrays offer limited direction finding and possible ranging of fifth-generation aircraft at tactically significant ranges in certain conditions. Radar directed weapons will continue to be the most capable and deadly weapons aviation must contend with for the foreseeable future.

This project provides a proof-of-concept for a program that generates a three-dimensional volume representative of threat radar performance, which will aid planners in developing routes that avoid or minimize exposure to these threats and improve understanding of other radar phenomena. This representation includes a basic atmosphere model that demonstrates the effects of refraction, a depiction of the shadow zone, and terrain-masking effects. Future development would allow inclusion of location-specific weather and simulation of specific threat radars, allowing near real-time evaluation of radar capabilities that greatly exceed the abilities of current analytical tools.

THIS PAGE INTENTIONALLY LEFT BLANK

TABLE OF CONTENTS

LIST OF FIGURES

LIST OF TABLES

THIS PAGE INTENTIONALLY LEFT BLANK

LIST OF ACRONYMS AND ABBREVIATIONS

3D	three-dimensional
A2AD	anti-access, area denial
AGL	above ground level
DMED	digital mean elevation data
DoD	Department of Defense
DTED	digital terrain elevation data
EGM96	Earth Gravitational Model 1996
EM	electromagnetic
EW	Electronic Warfare
ASR	air surveillance radar
GHz	gigahertz
GMTI	ground moving target indicator
GPS	Global Positioning System
GPU	graphics processing unit
GUI	graphical user interface
HTML	Hyper Text Markup Language
ICAO	International Civil Aviation Organization
LOS	line-of-sight
MBR	minimum bounding rectangle
MCAS	Marine Corps Air Station
MGRS	Military Grid Reference System
MHz	megahertz
MSL	mean sea level
NIST	National Institute of Standards
P_d	probability-of-detection
PRI	pulse repetition interval
PRF	pulse repetition frequency
R2P2	rapid response planning process
RCS	radar cross section
SAM	surface-to-air missile

SAR	synthetic aperture radar
TTR	target tracking radar
URL	uniform resource locator
UTM	Universal Trans Mercator
WGS-84	World Geodetic System 1984
X3D	Extensible 3D

ACKNOWLEDGMENTS

The number of individuals and organizations that have contributed to the success of this thesis is great; there is not enough space to name or thank them all properly here. The list ranges from the Marine Corps, which inexplicably decided that an unremarkable English major ought to study computer science, to all of my professors, who taught me literally everything I know in said domain, and everyone in between—especially my peers, who doggedly dragged me through the curriculum (particularly Automata).

First, I must thank my advisors, Loren Peitso and Dr. Don Brutzman, for their support of my passion project. For their patience with occasional spaghetti code, lengthy and verbose drafts, and my general dull-headedness, I am exceptionally grateful. Thank you, gentlemen.

To Dr. Sungmin Kwon, thank you for donating the time to teach me some very useful tricks. Your work served to drop several key puzzle pieces into place for this project, and I am very appreciative. I wish you the best of luck.

To my cohort, I can honestly say that I am honored to know each of you. You impress me with your experiences, knowledge, and heart. I have no doubt that you all will continue to do great things for this nation and succeed in any domain you find yourselves in. I look forward to crossing paths with you in the fleet or hearing about your successes from afar.

To my spiritual mentors, who reinvigorated my faith and never shied away from a good theological debate, I cannot say enough. Suffice it to say that “it is well with my soul,” where it was not before. Thank you.

Finally, to the cellist of my heartstrings—English does not have enough superlatives for what you do for me. Despite all the miles and time zones between us, I feel closer to you than ever. I can’t wait to see what you achieve and become as you enter the next phase of your life. I am humbled to be yours.

THIS PAGE INTENTIONALLY LEFT BLANK

I. INTRODUCTION

A. BACKGROUND

The purpose of this thesis is to demonstrate the viability of a squadron-level tool for visualizing physics-based environmentally correct threat radar envelopes. It must scale to work on standard laptops, render output within seconds, and depict the critical parameters of ground-based radars with greater fidelity and flexibility than existing tools, which often default to drawing simple circles or very coarse single-altitude masks on two-dimensional charts.

Radars, utilized for both early warning and directing surface-to-air fires, will only become more ubiquitous in future battlefields. Signal processing, phased array beam forming, and power output are all increasing in capability while simultaneously becoming cheaper and more common, increasing the range at which aircraft may be detected and tracked and increasing the lethality of anti-air weapon systems.

Newer low-observable (LO) aircraft have a limited ability to avoid detection by certain kinds of radars, but the vast majority of Navy and Marine Corps platforms will not be LO. Furthermore, even LO aircraft may be detected intermittently depending on radar frequency and aspect within certain ranges.

The capabilities of sophisticated radars must be understood, not overstated; for even the most capable adversary radars face hard physical limits. Terrain blocks RF emissions, preventing detection of aircraft masked by terrain features. Even in a notional sea level plane, the curvature of the Earth imposes a radar horizon that prevents detection of aircraft flying beyond it. Meteorological conditions further complicate radar capabilities through absorption, refraction, and reflection.

These limitations are critical – radars are the foundation of modern air defense and accurately visualizing where an aircraft will not be detected by a particular radar provides a host of valuable information. It allows routes to be planned that minimize risk and maximize surprise. This knowledge must be presented in a meaningful and timely manner to properly support tactical aviation—and in the face of rapidly increasing friendly and

threat capabilities, this presentation must be more nuanced than simply drawing a circle on a flat map.

To this end, a great deal of research has already been conducted. The principles through which a radar detects an aircraft are well understood and significant work has been done in the realm of modeling this event, to include simulations of radar performance against aircraft utilizing both time step and discrete event simulation with high-fidelity physics models (Cheng, 2016).

While this work is of inestimable usefulness at the strategic level, the granularity, specificity of required inputs, and computation cost make these solutions cumbersome for use at the tactical level. In a six-hour Marine Corps Rapid Response Planning Process (R2P2) cycle or other time-compressed environment, the amount of detail and specificity required to populate these models is unsupportable. A different approach is required.

This thesis will start with existing radar equations and standard atmospheric models. It will utilize these building blocks as the foundation of a system that will depict the capability of a radar in real-world terrain in three dimensions. The regions within which significant multipath and clutter impacts may occur will likewise be depicted. Initially, only a standard weather model will be available, but future iterations of the project will be able to incorporate climates that are more exotic.

Solving these initial problems is a first step towards future capabilities within the realm of mission planning, to include least-risk/shortest-time flight path recommendations, probability-of-detection simulation, and is further extensible to address electronic warfare concerns, notably noise jamming propagation.

B. LIMITATIONS

One of the challenges of projects of this scale is performing the necessary radar line of sight calculations. A simulation capable of depicting the detection volume of the most capable SAM systems and air search radars today must represent five-hundred square miles of area with varied terrain and an altitude block from sea-level to around fifty thousand feet.

To be useful in a tactical setting, a program must perform these computations with relevant speed. The user must be able to view and analyze the performance of the radar system from multiple different possible employment sites in the terrain without spending more than a reasonable number of seconds per render per threat system.

This is a non-trivial problem. Even a smaller volume consisting of a two-hundred square kilometer ground mesh contains over twenty-thousand polygons; a simple implementation of line of sight checks would require a test against each of these polygons, and take far too long to complete in a time-compressed setting (Koler & Shintel, 2017). This necessitates algorithmic efficiency and an acceptable level of approximation.

Due to the variety of specific frequencies, power outputs, signal processing techniques, and classification concerns, the demonstration system does not attempt to model specific radars. However, user selection of different radar parameters is allowed, permitting the use of classified parametrics on appropriately classified and protected systems.

The project does not attempt to model specific probabilities of detection. Due to the wide variety of platforms and the dependence on target aspect and speed, the project will only provide a general model of electromagnetic wave propagation, depicting the areas radar energy could reasonably be expected to reach, and not attempt to render how much energy reaches specific points or model a return trip to the emitter.

Atmospheric conditions have significant effects on radar propagation and specific programs are used by meteorology specialists within the Department of Defense (DoD) to perform atmospheric analysis. These models are exceptionally accurate but rely on time-sensitive measurements. The demonstration system will therefore not be designed to model a specific atmospheric condition or otherwise connect to external databases. Instead, it will present the radar capabilities for the U.S. Standard Atmosphere (defined in Chapter II, Section B) and humidity that conform to models within the DoD manual, *Modeling Climatic Data*. Increased parameterization is a high priority for future work as described in Chapter V.

THIS PAGE INTENTIONALLY LEFT BLANK

II. LITERATURE REVIEW

This section begins with descriptions of essential radar concepts, then proceeds into the characteristics of radar energy propagation and atmospheric effects. It will then discuss the factors that limit radar visibility, specifically radar horizon, multipath, and clutter. Finally, it will describe the models used to represent operational conditions and data formats.

A. KEY TERMS

1. Electromagnetic Waves

Electromagnetic (EM) waves are a combination of electric and magnetic oscillations that demonstrate a sinusoidal waveform. EM waves travel through space at the speed of light in a vacuum (defined in this document as the constant c, 3×10^8 meters per second) (Richards, Scheer, & Holm, 2010). Pertinent terms related to EM waves (and the frequency subset employed by radar) are described in 1.a through 1.d.

a. Wavelength

The wavelength (λ) is the physical space between corresponding points on the waveform, i.e. the distance from a wave's peak to the next peak. Some bodies classify radar waves by their wavelength, capturing bands with similar performance in the same category, e.g. millimeter wave radar or the ten-centimeter band (Richards, Scheer, & Holm, 2010).

b. Frequency

Frequency refers to the number of cycles a wave completes per second. It is the inverse of the wave's period, or the time taken for a wave to complete a single cycle. The most common frequencies employed by modern radars are between 300 megahertz (MHz) and 35 gigahertz (GHz), or 300 million cycles per second and 35 billion cycles per second respectively (Richards, Scheer, & Holm, 2010).

c. Phase

An arbitrary value that describes a wave's position along the waveform cycle at a given time. *Relative Phase* refers to the phase difference between two waves. A relative phase of zero refers to two waves that are in-phase with each other, i.e. all peaks and troughs are exactly aligned. Non-zero relative phases refer to waves that are out-of-phase. Two waves of the same amplitude that are 180 degrees out of phase will nullify each other (Richards, Scheer, & Holm, 2010).

d. Intensity

Intensity (*Q*) is defined as power per unit of area (watts per square meter). With respect to radar, intensity is calculated in two different forms, depending upon the distance from the notional emitter. The spherical form approximates the total radiated transmitted power over the surface of the sphere. At greater distances, the wavefront is traditionally approximated by a plane as noted in Figure 1 (Richards, Scheer, & Holm, 2010).

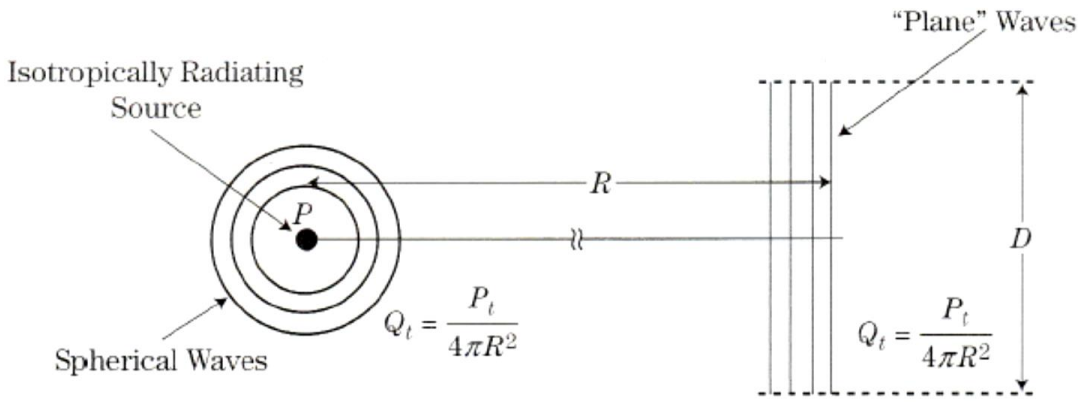

Figure 1. Isotropic and Planar Intensity. Source: Richards, Scheer, and Holm (2010).

Intensity is a key parameter required to calculate the radar's probability-of-detection (P_d). Unless the power that reaches a target is above the threshold of ambient and system noise, the object will remain undetected.

2. Radar

A radar is defined as "an electrical system that transmits radiofrequency electromagnetic waves toward a region of interest and receives and detects these EM waves when reflected from objects in that region" (Richards, Scheer, & Holm, 2010, p. 4). "Radar" was initially conceived as an acronym (RAdio Detection And Ranging) but has entered common usage and will not be capitalized per current convention.

There are many different kinds of radar; the manner in which the EM waveform is produced and shaped vary drastically across technology generations, however, the general principle remains consistent and is depicted in Figure 2. A transmitter produces the EM wave with an oscillator and uses a modulator to regulate the wave's duration. A waveguide transmits the generated wave to the antenna. The antenna then amplifies, shapes, and radiates the wave into the atmosphere. In the case of monostatic radars, the same antenna will then collect waves of a similar frequency and send them to the radar's receiver, which will pass the signal to the signal processor (Richards, Scheer, & Holm, 2010).

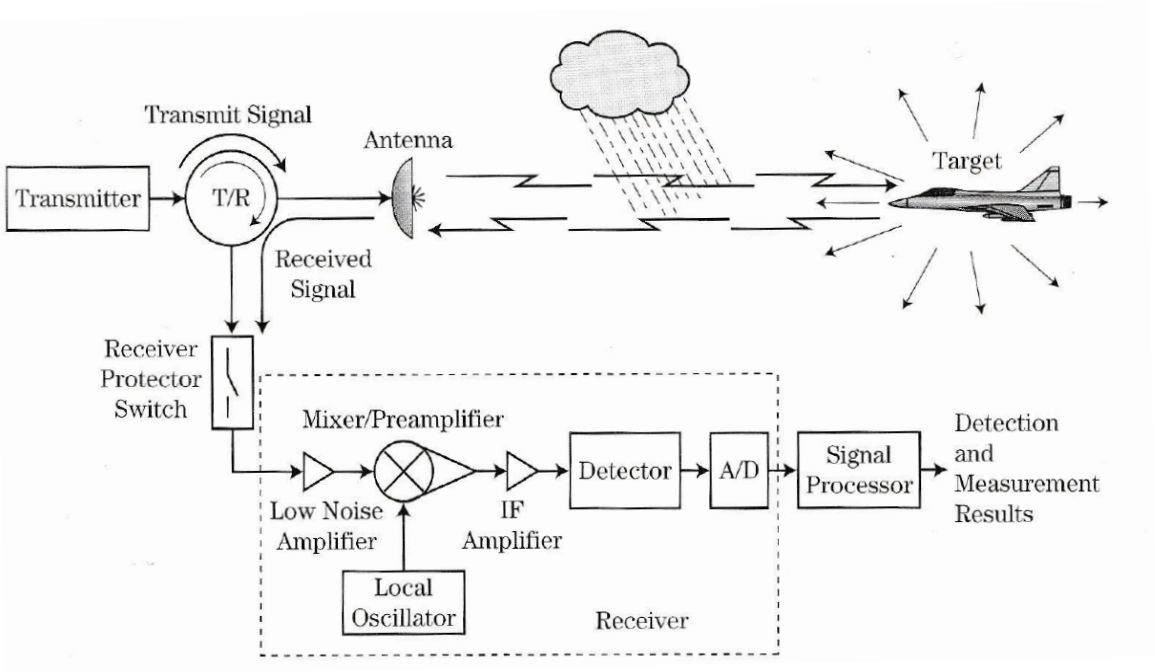

Figure 2. Radar Block Diagram. Source: Richards, Scheer, and Holm (2010).

Radars are classified by their parametrics, or the physical descriptions of their emitted EM waves, particularly by frequency or wavelength. Some of these key parameters are described in Sections 2.a through 2.g.

a. Bandwidth

Bandwidth refers to the breadth of the EM spectrum the radar is capable of operating within. Radars are then classified by the frequencies they are able to produce. A radar may be said to operate within an entire band but only is only capable of employing one or a few specific frequencies due to aperture and/or signal processing limitations.

A number of different organizations classify ranges of frequencies in "bands" defined in Appendix A. Frequencies within the same band have generally similar characteristics but the specific frequencies that delineate the bands are arbitrary; for instance a frequency 5 kilohertz below the D band will still behave similarly to frequencies at the bottom of the D band (Richards, Scheer, & Holm, 2010).

b. Beamwidth

Beamwidth is a measurement of the antenna's main beam, the angle across which it is designed to receive a return. Specifically, it is the measurement from one side of the beam, starting at which the emitted wave is at half power, to the opposite half-power point, as depicted in Figure 3 (Richards, Scheer, & Holm, 2010).

The main beam may have different horizontal and vertical components depending on the intended design of the antenna. For instance, height-finding radars are often designed to have a very narrow (accurate) vertical beamwidth in order to provide granular target elevation measurements, but a wide (inaccurate) horizontal beamwidth (Richards, Scheer, & Holm, 2010).

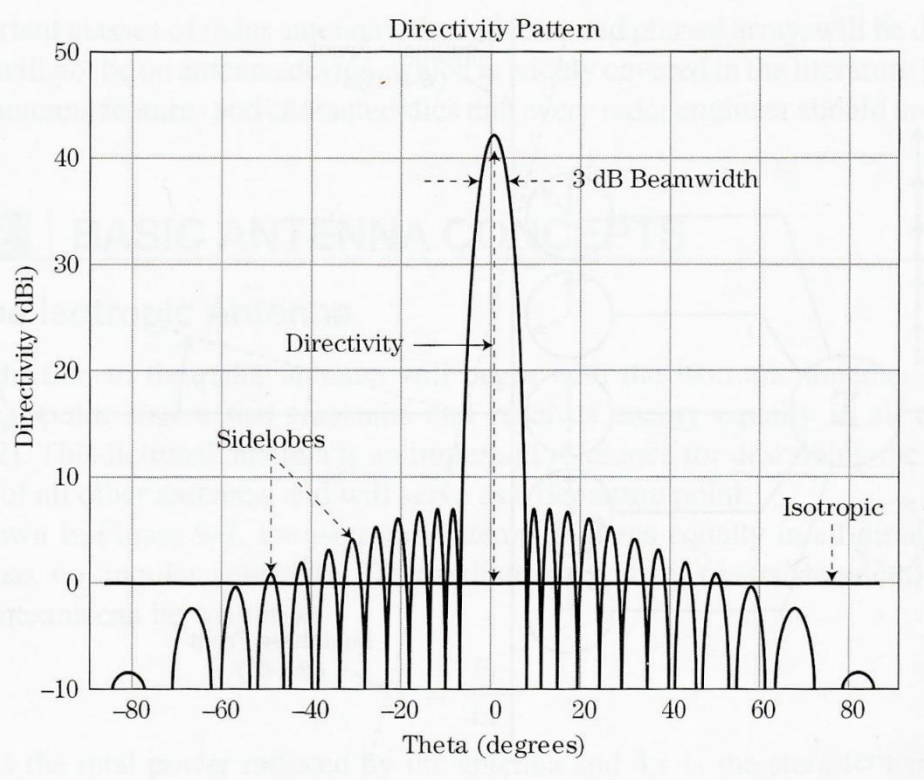

Figure 3. Beamwidth (Two-Dimensional). Source: Richards, Scheer, and Holm (2010).

It is important to note that the radar both emits and receives power from outside of the main lobe. Radar design generally assumes that received energy is from the main beam, even if it is possible for sidelobe or less than half power point energy to return. This is generally undesirable because sidelobe energy will often be interpreted as coming from the direction of the main lobe, reducing system accuracy and leaving the radar open to deception techniques. However, it does represent an efficient shorthand for depicting the limits for a radar's momentary field of view (Barton, 2005).

c. Pulse Width

Pulse width (PW) is a measurement of the time a radar spends transmitting during a single cycle. Monostatic radars cannot receive during this time. This value generally ranges between a nanosecond to a millisecond, depending on the purpose of the radar. By multiplying the pulse width by the speed of light, the linear distance traveled by the pulse

per transmit cycle may be deduced. For unmodulated pulses, this distance reflects the space between which two separate objects cannot be resolved. Generally, the more granular the application, the shorter the pulse width (Richards, Scheer, & Holm, 2010).

d. Pulse Repetition Interval

The pulse repetition interval (PRI) is a measurement of the length of time a radar takes to complete a single transmit and receive cycle. (Richards, Scheer, & Holm, 2010).

e. Pulse Repetition Frequency

The number of times a complete send/receive cycle takes place per second; calculated by taking the inverse of the PRI (Richards, Scheer, & Holm, 2010).

f. Unambiguous Range

Unambiguous range is defined by the maximum distance a transmitted wave can travel during a single PRI. While the radar would be capable of receiving a return from targets beyond this point, the system would generally have no way of determining whether the detecting pulse had been produced during that cycle or innumerable cycles before, producing an ambiguity in range (Richards, Scheer, & Holm, 2010).

Because of this, radars are often designed to not display detection information at distances in excess of the unambiguous range defined by the system's PRI, either in the form of a hard display limit or through software. Modern radars may use other techniques to encode identifying information within each pulse to allow for differentiation of returning pulses, increasing the unambiguous range (Barton, 2005).

g. Resolution cell

The indivisible unit that represents a radar system's fidelity is known as the radar resolution cell (RRC), visually depicted in Figure 4. The RRC is a volume with upper/lower and left/right limits defined by the antenna's horizontal (Θ) and vertical (ϕ) beamwidths. The volume's outward and inward faces are a function of the radar's pulse width, the speed of light (C) times the radar's PRI (τ) (Richards, Scheer, & Holm, 2010).

Within each cell, the amount of returned energy from a pulse determines whether the radar signal processor marks the presence or absence of a target. If the returned energy is below the ambient system noise, the cell will be considered empty (Barton, 2005).

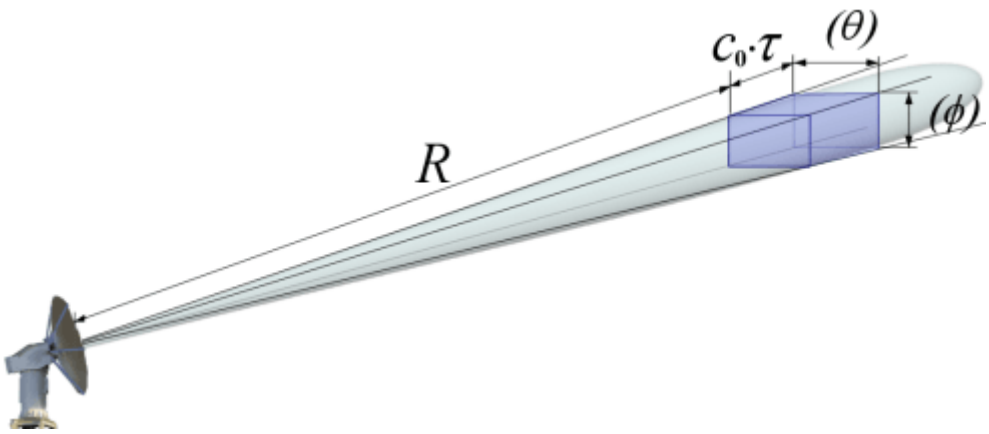

Figure 4. Resolution Cell. Source: Wolff (n.d.).

It is important to note that unlike the equally sized pixels used in describing digital screen resolution, a radar's pulse wavefront expands as the distance from the antenna increases, meaning that a radar's RRC height and width will increase proportionate to the increase in a sphere's surface area relative to its radius (Barton, 2005). At significant distances from the emitter, the leading edge of the wavefront is often treated as linear instead of spherical (Richards, Scheer, & Holm, 2010).

B. RADAR LIMITATIONS

EM waves traveling through the Earth's atmosphere are affected by a number of phenomenon. While these effects will vary based on the local weather, they will always be present in some form or another. Furthermore, when radars are operated on Earth, they will be affected by line-of-sight limitations (Richards, Scheer, & Holm, 2010).

1. Atmospheric Attenuation

Attenuation refers to the loss of energy experienced by EM waves proceeding through the atmosphere. There are two primary factors: absorption and scattering. Together these constitute the greatest source of energy loss in most circumstances (Richards, Scheer,

& Holm, 2010). Absorption occurs when the wave contacts particles and some of the wave's energy is converted to heat within the particle. Scattering refers to the loss that occurs when the EM energy is reflected off of the particle and in directions away from the receiver (Richards, Scheer, & Holm, 2010).

Because both of these features are functions of the density of the conducting medium, they are proportionately greater the denser the atmosphere. Humidity, precipitation, and any other particulates in the beam path likewise serve to increase these effects (Richards, Scheer, & Holm, 2010).

2. Refraction

Refraction is defined as "the change in direction of travel of radio waves due to a spatial change in the index of refraction" (Richards, Scheer, & Holm, 2010, p. 130). The index is a ratio of the speed of light in a vacuum and the speed of the wave in the atmosphere. Like atmospheric attenuation, the refractive index is a function of atmospheric density, and generally decreases as altitude increases. Water content also affects the amount of refraction (Richards, Scheer, & Holm, 2010).

Refraction comes in two varieties, standard and anomalous. Standard refraction effectively curves radar energy slightly downward at an approximately linear rate as altitude increases. This effect is not negligible; assuming a constant linear rate, refraction increases the Earth's effective radius by a factor of 4/3 (Richards, Scheer, & Holm, 2010). Figure 5 depicts both varieties of refraction.

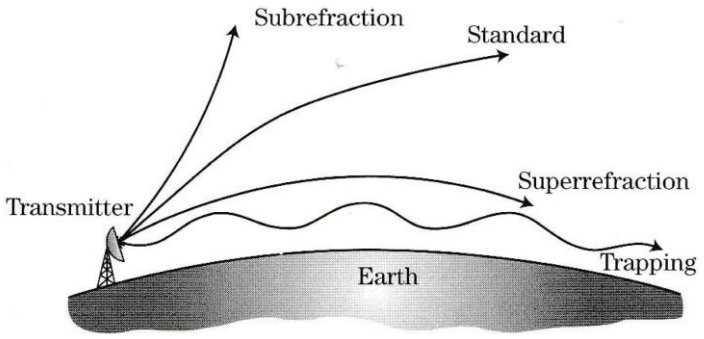

Figure 5. Refraction Types. Source: Richards, Scheer, and Holm (2010).

Anomalous refraction includes a number of behaviors that deviate from the linear refractive index model. This includes atmosphere types that cause a wave to curve away from the Earth's surface (subrefraction), bend towards the Earth at a significantly greater rate (superrefraction), or trapping EM energy parallel to the surface (ducting) (Richards, Scheer, & Holm, 2010).

The factors that influence EM refraction within the atmosphere are humidity, temperature, and density, which all experience both the greatest variability and presence at low altitudes. A specific sub type of the refraction phenomena is noted in the following section.

3. Ducting

Ducting is often caused by temperature inversions, defined as the atmospheric state in which a warmer mass of air is located above a colder mass or when humidity decreases in proportion to altitude. The common effect is to redirect a greater proportion of the EM energy in a channel, or duct, along the surface, while producing shadow zones at higher altitudes. The radar operator is generally unable to discern that this phenomenon is occurring (Richards, Scheer, & Holm, 2010). Figure 6 presents a standard ducting profile.

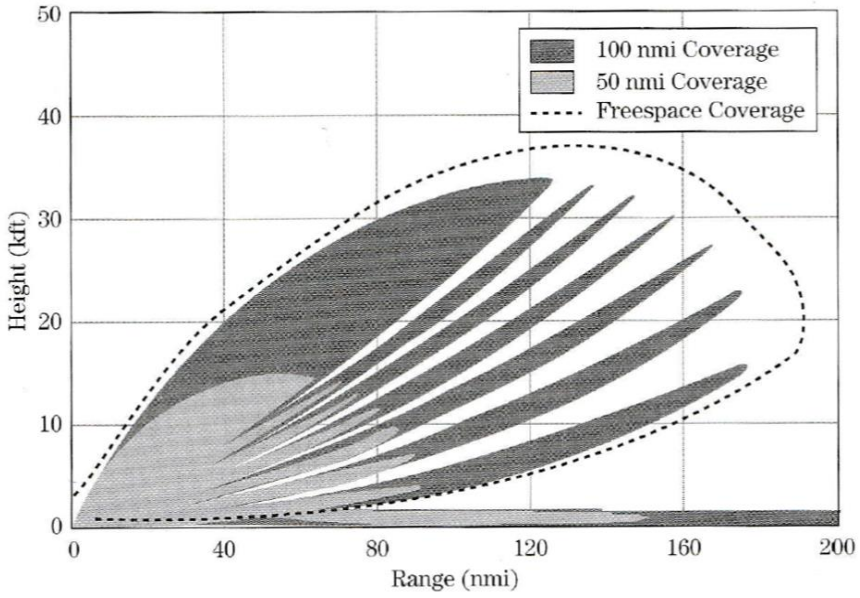

Figure 6. Ducting. Source: Richards, Scheer, and Holm (2010).

While ducts are usually small (10 to 20 meters in general cases, up to 200 meters at the maximum), they can degrade a system's ability to generate a consistent target-quality track as a target intermittently enters and leaves the duct (Richards, Scheer, & Holm, 2010).

4. Radar Horizon

The curvature of the Earth will make it unlikely that EM energy may return from a target below the line tangent to the curve of the earth's surface from the wave's origin. This line is the radar horizon line. The area below this line is referred to as the shadow zone, as depicted in Figure 7 (Richards, Scheer, & Holm, 2010).

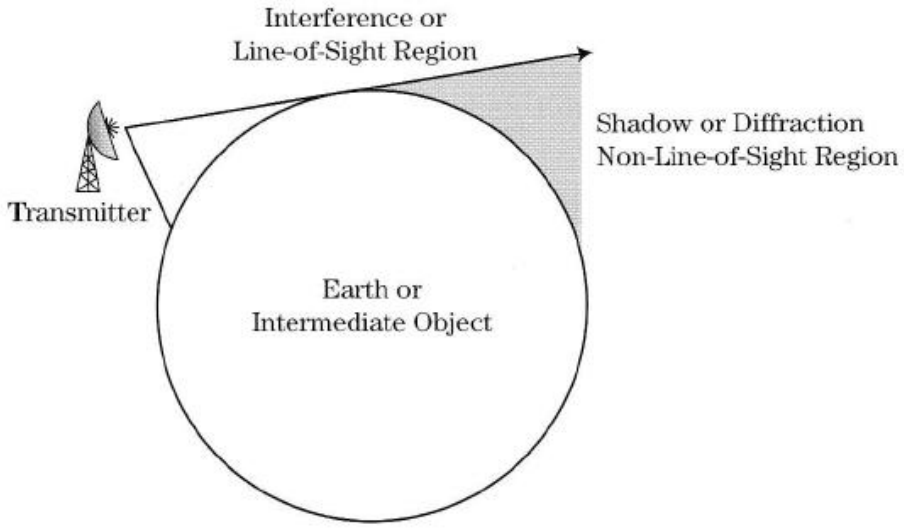

Figure 7. Simple Radar Horizon. Source: Richards, Scheer, and Holm (2010).

In standard conditions radar waves bend downward, effectively extending their travel beyond the horizon point of the same ray within a vacuum. Therefore a simple straight-line between points, often used for visible light line of sight calculations, does not adequately reflect the radar line of sight (Richards, Scheer, & Holm, 2010).

5. Multipath and Clutter

Multipath occurs when an emitted signal returns to the receiver by two or more paths. The majority of the antenna's main beam will bounce off the intended target but

energy from the same pulse may be reflected and returned off of terrain or other objects as depicted in Figure 8. This causes either constructive or destructive interference and can create "ghost" contacts and errors in both range and azimuth (Avionics Department, 2013). Multipath effects are strongest in the region between the radar horizon line and 0.6 beamwidths above (Barton, 2005).

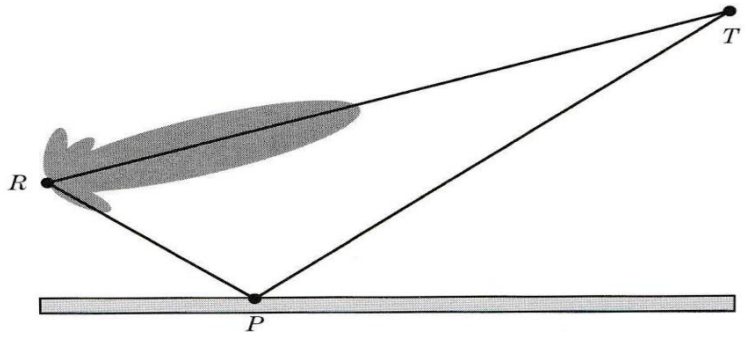

Figure 8. Multipath. Source: Richards, Scheer, and Holm (2010).

Clutter is defined as any undesired reflected radar returns. It is produced by radar reflections from clouds, terrain, waves, trees, and other such objects that the radar does not intend to detect (Avionics Department, 2013). There are many radar techniques to compensate for clutter that are outside the scope of the model; in general, aircraft within the multipath region should not be considered undetectable (Barton, 2005). However, it is still important to depict the locations where multipath and ground clutter effects are likely to degrade a radar's performance. Figure 9 depicts a high clutter situation.

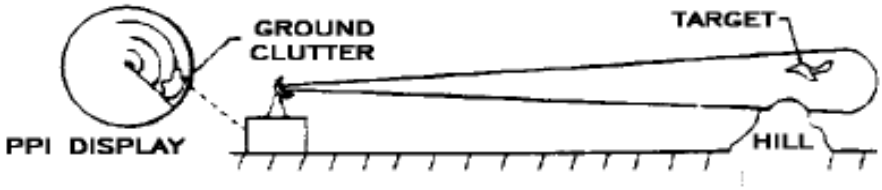

Figure 9. Clutter. Source: Avionics Department (2013).

C. MODELS AND MEASUREMENTS

1. The Standard Atmosphere

A number of organizations have published atmospheric models that attempt to produce a steady-state representation of the Earth's atmosphere. The U.S. Standard Atmosphere, the Standard Atmosphere of the International Civil Aviation Organization (ICAO), and the International Standard Atmosphere, the three most common models, differ only in the atmospheric regions above 30 kilometers (Richards, Scheer, & Holm, 2010). All of the models provide information in one-kilometer blocks.

For altitudes relevant to Naval Aviation, defined in this document by the unclassified operational ceiling of the F-35 family of aircraft, ~15 kilometers (Air Combat Command Public Affairs Office, 2014), the differences between the models are negligible (Richards, Scheer, & Holm, 2010). The pressure and temperature of the standard atmosphere is depicted in tabular form in Appendix B.

2. Humidity

In general, humidity is greatest near sea level, and decreases exponentially as altitude increases. At altitudes above 15km, due to the low total pressure and low temperatures, water vapor presence is minimal (less than 0.001 hPa) and has minimal effects on refraction (Palchetti, Bianchini, Carli, Cortesi, & Del Bianco, 2008).

Humidity is expressed in different ways, but the absolute unit format used to calculate atmospheric refraction is partial pressure, the amount of pressure contributed by a single component molecule in a mixture (Bell, 2012). Two different representative humidity charts are depicted in Appendix C, one which represents a standard day, typified by an exponential decrease in partial pressure of water as altitude increases, and a second which represents an inversion at low altitude, which greatly increases refractive effects.

3. Radar Horizon Approximations

The next section describes radar horizon approximation methods. Means of deriving a simple geometric path and a curved path that accounts for atmospheric refraction

(graphically depicted in Figure 10) are defined, with descriptions of their assumptions about atmospheric conditions.

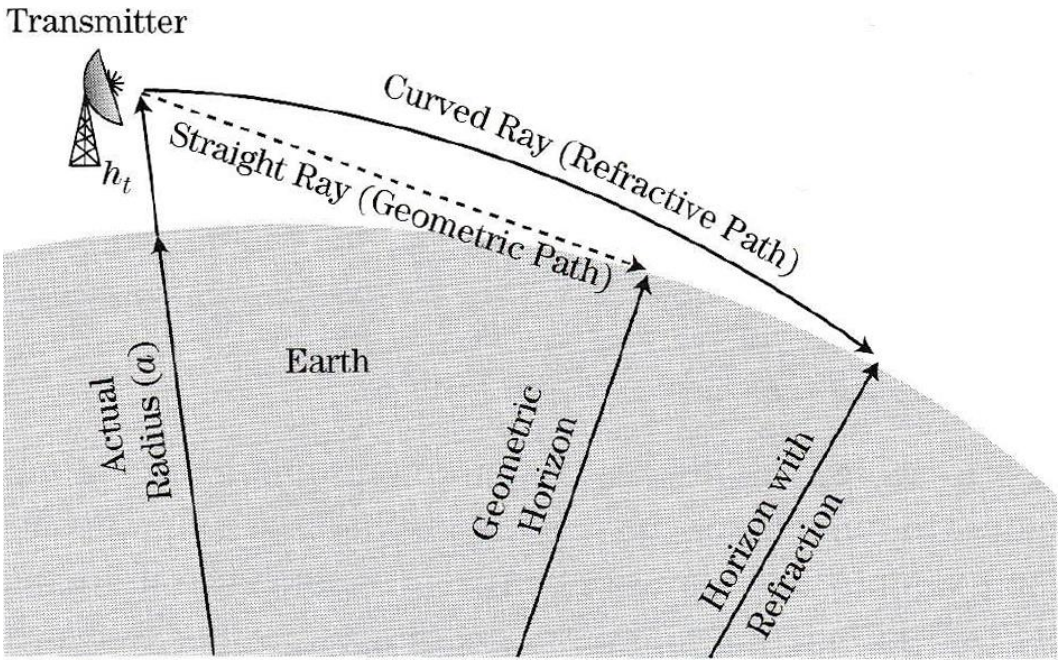

Figure 10. Radar Horizon: Geometric and Standard Models. Source: Richards, Scheer, and Holm (2010).

a. Geometric Approximation

The most basic approximation uses the Pythagorean Theorem to define the last point on a circle visible to an observer at a noted height, where the Earth's radius is used as the leg of a right triangle, with the hypotenuse's length being defined as the Earth's radius (*R)* plus the height of the observer (*h)*. This leaves the final leg of the triangle (*d*) as the geometric path, as depicted in Figure 10 (Plait, 2009).

$$R^2 + d^2 = \left(R + h \right)^2$$

Simplifying this equation and solving for the geometric path (*d*) yields the following formula (Plait, 2009):

$$d = \sqrt{h\left(2*R + h \right)}$$

This is the least accurate means of approximating EM propagation; as depicted in Figure 10, there is a significant difference between the geometric and refractive horizons.

b. The Four-Thirds Approximation

The Four-Thirds Approximation builds on the simple Geometric Approximation while fundamentally using the same method to achieve a result. It summarizes refraction, ducting, and meteorological factors into a single constant that results in a modification of the Earth's radius by a factor of 4/3. This new radius is then used in the same Pythagorean Theorem. (Barton, 2005).

$$d = \sqrt{h\left(2 * \left(\frac{4}{3}\right) * R + h\right)}$$

This represents an improvement over the Geometric Approximation, but it assumes constant atmospheric conditions, and assumes that the rate of refraction remains linear.

c. Concentric Circles Approximation

A more accurate model of the atmosphere consists of a number of concentric circles of increasing radii, each of which may have a different effect on radar waves that pass through them (Richards, Scheer, & Holm, 2010).

The formula is a form of Snell's Law in which the index of refraction for a given atmosphere block (n_x) is multiplied by the radius of the Earth at that altitude (r_x) and the cosine of the angle of the incident wave (a_x). This is equal to the product of the adjacent index of refraction (n_y), radius (r_y), and incident angle (a_y). By solving for a_y, the wave's next incident angle may be found, and so on, as depicted in Figure 11.

$$n_x r_x \cos(a_x) = n_y r_y \cos(a_y) = n_z r_z \cos(a_z) = \ldots$$

Calculating the index of refraction (n) remains contingent upon atmospheric pressure, humidity, and temperature. The most accessible equation used to solve for the refractive index is the Smith-Weintraub equation, in which the amount of refraction by the primary components of the atmosphere are computed separately and then summed (Mangum & Wallace, 2015).

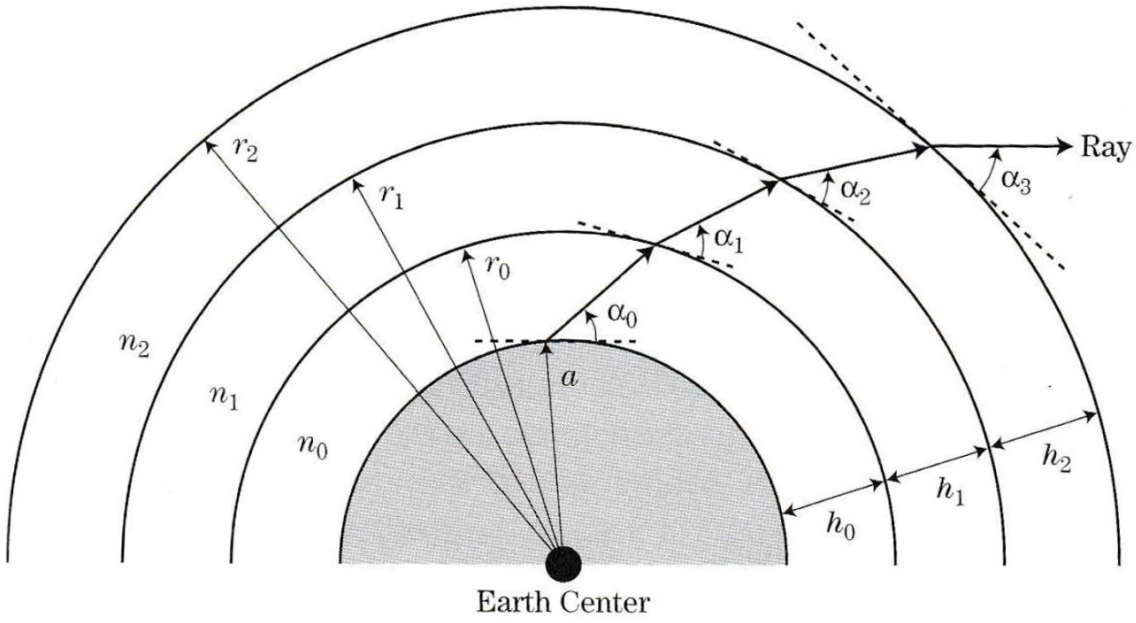

Figure 11. Snell's Law, Isotropic Model. Source: Richards, Scheer, and Holm (2010).

The refractivity of the "dry" components (N_d), primarily oxygen and nitrogen, are defined by multiplying a constant k_1 with the proportion of partial pressure of the dry gases over the temperature This value is then summed with the refractivities for the carbon dioxide (N_c) and "wet" (N_w) components, each of which has a respective constant k_2 and k_3 (Mangum & Wallace, 2015).

$$N_d = k_1\left(\frac{P_d}{T}\right)$$

$$N_w = k_2\left(\frac{P_w}{T}\right) + k_3\left(\frac{P_w}{T^2}\right)$$

$$N_c = k_4\left(\frac{P_c}{T}\right)$$

This method encounters some inaccuracy when EM frequencies are close to or within the absorption frequencies for water and oxygen (Mangum & Wallace, 2015). However, search, tracking, and engagement radars are generally designed to avoid these high-absorption frequencies due to their inefficiency and high clutter in radar applications (Richards, Scheer, & Holm, 2010).

D. TERRAIN REPRESENTATION

Modeling terrain is one of the key features of representing a radar detection volume with any tactical utility. Most existing solutions utilize Digital Terrain Elevation Data (DTED) standards (Durland, 2009).

Digital Terrain Elevation Data (DTED) is the standard elevation mapping format utilized within the DoD. It is a geographic matrix of elevation measurements mapped to latitude and longitude. DTED remains the standard elevation format for use in mission planning within the aviation and communication communities.

Before continuing with any further discussion of measuring terrain elevation, a baseline must be established. Within geodesy, mean sea level (MSL) is this reference. The most common model is the World Geodetic System 1984 (WGS-84) reference ellipsoid with corrected values from the Earth Gravitational Model 1996 (EGM96), which serves as the zero-elevation reference within DTED. In order to maintain accuracy in using DTED, the globe model must include the correct ellipsoid height value at the DTED elevation measurement point (Durland, 2009).

DTED information comes in three classes, 0, 1, and 2. Level 0 is the least detailed, with measurements every 30 arc seconds, approximately every 900 meters (measured at the equator). Level 1 is spaced every 3 arc seconds. Level 2 is the most precise, with measurements plotted every 1 arc second, or approximately every 30 meters at the equator.

Elevation data is contained in files with `.dt0`, `.dt1`, or `.dt2` extensions. Each file consists of a single cell, which represents a 1 degree of latitude by 1 degree of longitude square, roughly 60 by 60 nautical miles. (Leary, 1995). The measurement posts are denoted by the intersections of rows and columns within the file (NIMA, 2000).

Each `.dt<x>` file has an associated Digital Mean Elevation Data (DMED) text file that contains tabular information for each 15-minute-by-15-minute section of the associated one degree by one-degree cells. The file is broken into 394 character chunks. The first chunk defines the minimum bounding rectangle (MBR) for all the cells represented in the associated `.dt<x>` file. The next 394-character segment contains the information for the most southwesterly 1-degree-by-1-degree cell in the MBR. The next

394-character segment reflects the 1-degree cell directly north of the prior record, and so on to the top of the MBR, at which point the next record starts at the bottom of the adjacent easterly column, until the entirety of the MBR is represented (NIMA, 2000).

The rest of the `.dt<x>` file consists of hexadecimal values representing the actual elevation post values themselves, with each delimited value representing the height above the local Earth radius in meters (NIMA, 2000).

THIS PAGE INTENTIONALLY LEFT BLANK

III. METHODOLOGY

Visually depicting the radar detection volume requires that a number of subtasks be completed. EM behavior models must be developed and then implemented within a suitable simulation environment. These must then be conformed to a spherical coordinate system to map to the correct point on the Earth's surface.

A. EM BEHAVIOR MODELING

1. Radar Resolution Cell

The fundamental building block of the simulation is the RRC. Per the definition in Chapter II, Section A, the RRC is a three-dimensional object defined in depth by the radar's pulse width, in width by the horizontal beamwidth, and height by the vertical beamwidth. These parameters are all input by the user.

a. RRC Shape and Dimensions

When simulating the entire volume of space radar energy may propagate to, the specific, instantaneous RRC volume is not important because the visualization is designed to represent all the locations where radar energy may reach and not individual snapshots of a specific radar at a specific time. Utilizing RRCs also avoids the issues of scale noted in Chapter II, Section D by reducing the granularity of the problem, changing the likely time required to compute from hours or days to seconds or minutes (Koler & Shintel, 2017).

The technically correct shape for an RRC is a truncated pyramid, as shown in Figure 4 (Richards, Scheer, & Holm, 2010). However, to increase efficiency in rendering and calculation, the RRC is approximated as a rectangular prism instead of a truncated pyramid.

Additionally, given that beamwidth measurements only reflects the half-power point out of the main beam, and not the point at which no radar energy is emitted, the "edges" of the RRC are not as harshly defined as depicted in Figure 12 (Richards, Scheer, & Holm, 2010). Approximating precise power output is outside the scope of this project.

For planners concerned with finding an unobserved route near a radar, the assumption must be made that the exact, moment-to-moment orientation of the radar cannot be known. Instead, the concern is defining the entirety of the volume, because the radar could feasibly scan the entirety of said volume within seconds.

Therefore, the RRCs depicted in the simulation are calculated from their leading edge, as shown in Figure 12. The center point is determined by multiplying the pulse width (τ) by the number of cells traversed, effectively providing the amount of distance traveled by the EM energy. From this value, the tangent of the horizontal (Θ) and vertical (Φ) beamwidths are multiplied by the amount of distance traveled to find the length of the respective side. This rendering corresponds to the planar model of propagation described in Chapter II, Section A.

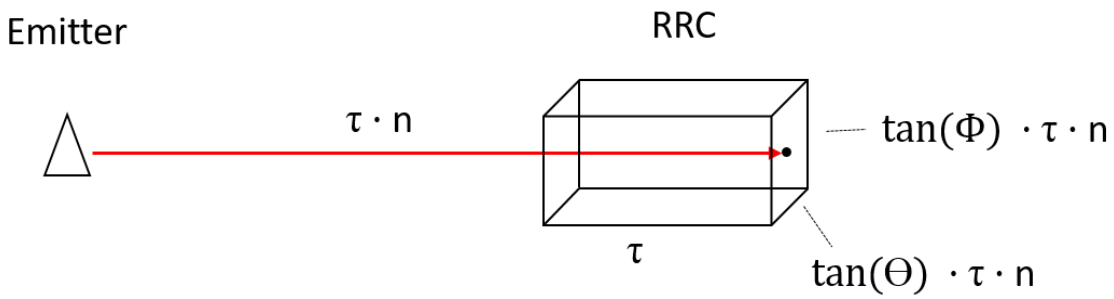

Figure 12. Radar Resolution Cell Approximation

Note that this is effectively the greatest extent of the RRC's height and width. A more accurate (and significantly more costly) method to represent the RRC is measuring the distance value twice: once at the closest point or trailing edge of the cell and again one pulsewidth further at the leading edge, and then joining the corner points to form the isosceles trapezoid for the truncated pyramid approximation. This approximation is acceptable given the goals of the project and requirement for speed in computation. Slight over-estimation of approximated RRCs are irrelevant considering the ultimate goal of presenting the entirety of the volume.

b. Forming a Beam from RRCs

By placing a number of RRCs end-to-end, the entire path of a radar beam is approximated, with each subsequent RRC accounting for the slightly greater distance from the emitter as shown in Figure 13.

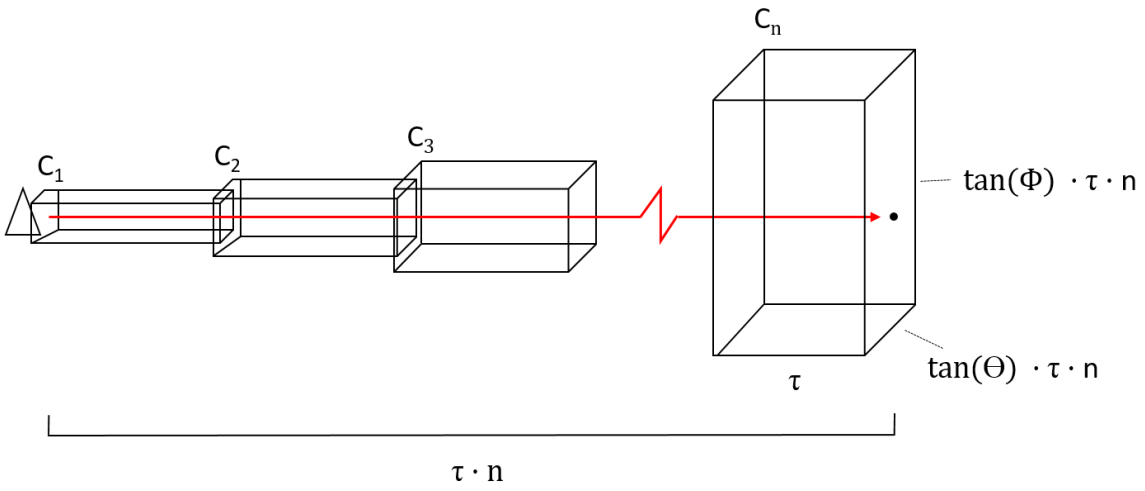

Figure 13. Beam Composed of Multiple RRCs

c. Naming RRCs

In order to efficiently reference the thousands of RRCs that are required to represent the radar detection envelope, each RRC must have a distinct and descriptive name, which consists of the azimuth measure of the beam it is a part of, its angle relative to the horizon in degrees as described by Snell's Law, and its numerical order in the beam.

2. Atmospheric Conditions

The next issue is simulating the relevant atmospheric conditions affecting EM wave refraction, specifically temperature, dry pressure, and wet pressure (humidity) as described in Chapter II, Section B.

Values for each condition are stored in lists ordered by altitude. To find the value of an atmospheric condition at a specified height, the two nearest round values are used to interpolate an intermediate value for use in calculating refraction.

This assumes that the traits of Earth's atmosphere at each altitude will be the same for every latitude and longitude. This does not account for weather fronts, climatic regions, or other disparities that are present between the same altitudes at different geographic locations. Incorporating a more accurate meteorological model is outside the scope of the project. This assumption in particular will likely produce the most divergence from real-world performance.

Three separate humidity models were used, two of which are annotated in Appendix C. The first model represents a wet climate, the second a dry climate with a low altitude temperature inversion, and the third is a constant zero to demonstrate the properties of temperature and pressure alone.

3. Calculating the Incident Angle

The atmosphere approximation described in Chapter II, Section C describing the circular version of Snell's Law. Calculating the N value requires humidity, temperature, and pressure, which may be derived from the standards described. From the basic formulation:

$$n_x r_x \cos(a_x) = n_y r_y \cos(a_y) = n_z r_z \cos(a_z) = \ldots$$

Starting from an origin, where the incident angle (a_x) is known, the incident angle of the next cell (a_y) may be solved for via:

$$a_y = \arccos\left(\frac{n_x r_x \cos(a_x)}{n_y r_y} \right)$$

By this means, the path of the beam as it travels away from the emitter may be incrementally described. Instead of propagating in a straight line as depicted in Figure 13, the new incident angle (a_n) for the next segment of the beam is calculated at the leading edge of the prior beam using the a_y formulation of Snell's Law, as depicted in Figure 14.

It is important to note that one of the most basic radar parameters, operating frequency, is accounted for in this equation. Frequency, were it to be included, would be present on both sides of the equation, and, given that it remains nearly identical from one step to the next, cancels itself out (Richards, Scheer, & Holm, 2010).

Furthermore, because intensity is not modeled, atmospheric attenuation is not included in calculating the effects of the atmosphere on wave propagation. All waves are described as proceeding to their unambiguous range and then ceasing propagation.

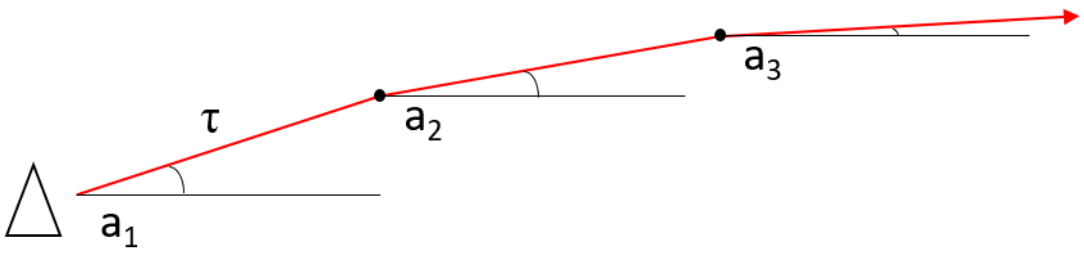

Figure 14. Linearly Approximated Beam Propagation

For each segment on this line, a corresponding RRC may be generated as depicted in Figure 15. In this manner, a single beam's path from the emitter to the radar's unambiguous range may be depicted.

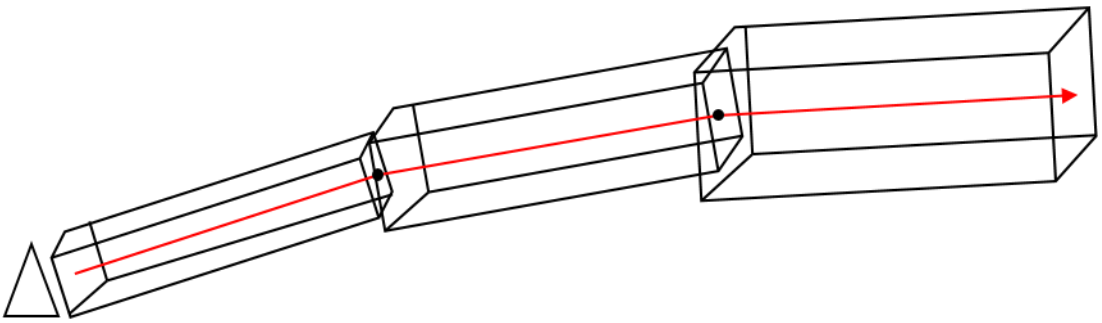

Figure 15. Segmented RRCs

4. Partitioning the Sky

At this point, the simulation must depict a radar's ability to cover the entirety of the sky both in azimuth and elevation. Because angles are continuous, an infinite number of beams are possible. To simplify, while still representing a radar's ability to cover the entirety of the sky, the next beam is assumed to radiate one horizontal beamwidth (Θ) clockwise to the prior beam as shown in Figure 16.

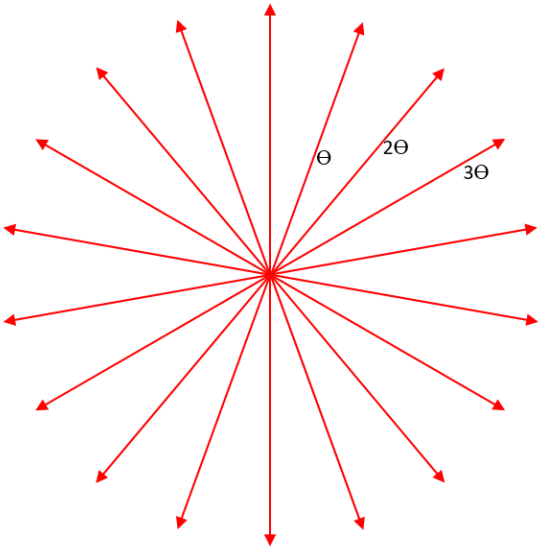

Figure 16. Rotational Coverage

RRCs are then calculated along each of these beams out to the unambiguous range as demonstrated in Figure 17. Note that the cells appear to overlap extensively, as the proportion between cell width and pulsewidth (cell depth) increases, the effect is greatly reduced.

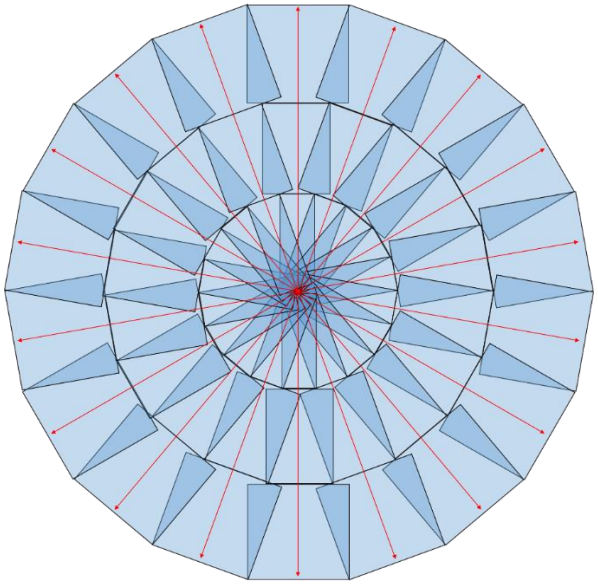

Figure 17. RRC Coverage Along Each Beam

The process is then repeated for elevation, with the above beam directed one vertical beamwidth higher than the one below. This allows for full coverage of the isotropic expansion model of propagation.

5. EM Wave Collision with Terrain

Because EM energy cannot pass through terrain, in the simulation a beam effectively ends when it comes into contact with the earth's surface. Terrain collisions are detected by comparing the altitude of a point within the cell with the height of the terrain at the same geographic position. If the cell point is lower than the terrain altitude, a collision occurs, and the cell is marked in a different color, and no further cells within that beam are drawn.

This does not account for the tendency of some frequencies of EM energy to curve around terrain features in some cases (Richards, Scheer, & Holm, 2010). This omission is acceptable because modeling specific frequencies is outside the scope of the model.

The program references elevation files in the DTED format (documented in Chapter II, Section D) for the specified latitude and longitude. The hexadecimal values in the DTED files are converted to an array of post values by a MATLAB script (Tung, 2009). In order to reduce the size of the array, the number of posts were down-sampled to a quarter of a million. Even with the down-sampling, testing every point within a cell is computationally costly; instead, a number of adjacent points are evaluated, based on distance from the emitter.

6. Multipath and Clutter

As described in Chapter II, Section B, multipath and clutter are most notable within one vertical beamwidth of the Earth's surface, due to the reflections and perturbations caused by EM energy within the beam being reflected and absorbed unpredictably during contact with the ground. This effect is minor once the half-power point of the beam no longer contacts the surface (Richards, Scheer, & Holm, 2010).

For this reason, RRCs that are within 0.6 beamwidths of the Earth's surface are depicted in a different color, to reflect degraded signal clarity. Because of the vast

differences in radar signal processing capability and clutter compensation techniques, any more specificity of the effects in these regions would not reflect the broadest spectrum of radars; the intent of marking these cells differently is to only represent the greater clutter and multipath effects present near the horizon compared to other cells.

B. GEODESY

The techniques described in Chapter III, Section A are completed within a traditional Cartesian coordinate system, which describes object location in terms of X, Y, and Z components. This is efficient for describing EM propagation, but translation to geographic coordinates in latitude, longitude, altitude format is necessary for comparison with DTED data, proper import into full-scale Earth models, and for human readability.

1. Earth Depiction

In current mission planning tools, the Earth is generally represented as a 2D projection. This is intuitive for human readability, but for aviation-relevant ranges, correctly representing the horizon issues posed by the reality of a spherical globe is an important design choice.

This presents two alternatives. If the Earth's surface is represented by a plane, then the radar waves must be depicted as curving upward to reflect the shadow zone. Alternatively, the Earth may be depicted as an oblate spheroid (per the WGS-84 standard described in Chapter III, Section D) and radar waves may be depicted as traveling straight (before refraction).

For computational simplicity and fidelity in graphical representation, the oblate spheroid Earth depiction was selected. This allows the radar propagation calculations described in Chapter III, Section A to be implemented as-is without additional modification to match EM line-of-sight and supports better integration with modern 3D Earth models.

The WGS-84 standard defines two relevant constants for computing the radius of the Earth at any given latitude ($r(\theta)$): the radius of the Earth at the equator (a) and the flattening value (f), a constant that describes the amount of z-axis compression compared

to a perfect sphere. The radius at any given latitude (θ) may be defined by the following equation (Sandwell, 2002):

$$r(\theta) = a\left(1 - f\left(\sin\theta\right)^2\right)$$

2. Coordinate Format Translation

Given the decision to represent the Earth as a sphere, the vector math described in Chapter III, Section A must be translated into spherical coordinates to test terrain and weather impacts. They then must be translated back into vector coordinates to correspond to the development environment.

a. Vector to Geocoordinate

Based on the local Earth radii (r_l) calculated per III.B.1 III, Section B, the conversion between vector coordinates and latitude and longitude becomes possible through trigonometric functions. Converting latitude, longitude, and altitude into vector coordinates (x, y, z) is performed via the following formulae:

$$x = \left(r_l + altitude\right) * \cos\left(latitude\right) * \cos\left(longitude\right)$$
$$y = \left(r_l + altitude\right) * \sin\left(latitude\right)$$
$$z = \left(r_l + altitude\right) * \cos\left(latitude\right) * \sin\left(longitude\right)$$

b. Geocoordinate to Vector

The conversion from vector coordinates to latitude, longitude, and altitude is accomplished similarly, by first calculating the local radius by the square root of the sum of the squares of the vector components:

$$r = \sqrt{x^2 + y^2 + z^2}$$

Subsequently, the latitude and longitude are calculated with trigonometry functions:

$$latitude = \arcsin\left(\frac{y}{r}\right)$$
$$longitude = \arctan 2\left(z, x\right)$$

Altitude is then derived by subtracting the Earth's radius at the calculated latitude from the local radius.

c. Altitude Translation

To correctly determine which altitude layer the beams exist within, and whether the beam will collide with terrain, the vector Y component must be converted into altitude (A_n) above a latitude/longitude, as depicted in Figure 18.

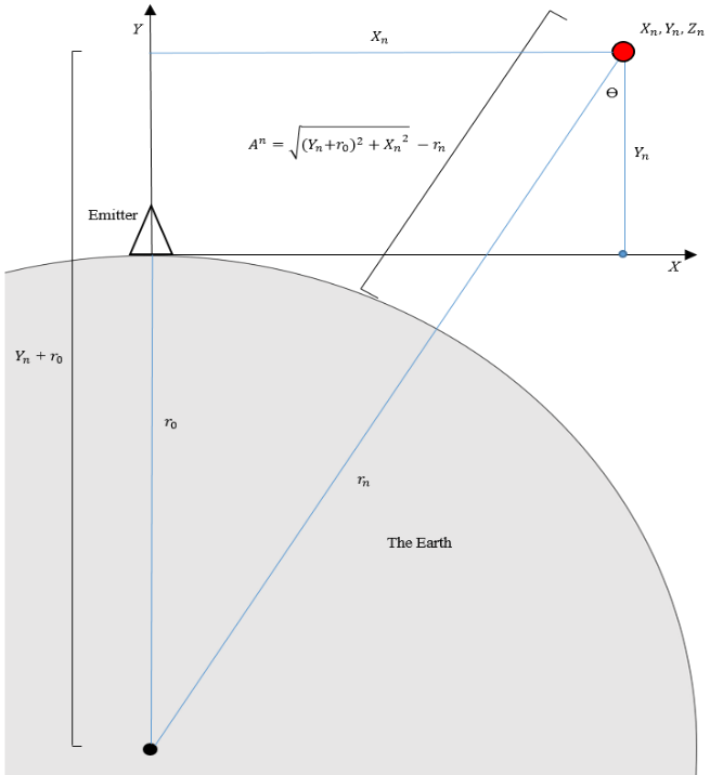

Figure 18. Converting from Vector Y to Altitude

By using the Pythagorean Theorem to solve for the hypotenuse of the right triangle made by the X component (X_n) and the sum of the Y component (Y_n) and the Earth's radius at the emitter (r_0), and then subtracting the Earth's radius at the target latitude and longitude (r_n), the true altitude above the Earth's surface (A_n) may be derived (Sandwell, 2002).

$$A_n = \sqrt{(Y_n + r_0)^2 + X_n{}^2} - r_n$$

This allows for accurate altitude parameter selection for use in Snell's Law as described in Chapter III, Section A.

C. UNITY3D SOFTWARE PACKAGE

Graphically presenting the models described in Chapter III, Section A is the best demonstration of the project's value, and essential to the key goal of producing an early approximation of a tactical-level tool to graphically depict radar detection envelopes. In this scenario, the platform that calculates and renders the model is central to both the user experience and the validation that the approximation model is functional.

Out of many capable options, Unity3D was selected to be the simulation platform due to its simplicity, accessibility, and open source nature. While Unity3D is generally used as a graphics engine for video games, its large, active user base and easy integration of physics-based behaviors made it a natural choice for this project. Furthermore, it features intuitive coding support and performs well on consumer-level laptops.

The project consists of a Unity scene, populated with objects representing the radar and its associated RRCs. All of these objects are created and manipulated from within the Unity3D graphical user interface (GUI). These objects are then associated with script files composed in a text editor. These files contain the equations described in Chapter III, Section A and all of the instructions for the Unity3D physics engine. The Unity3D interface is described in greater detail in Appendix D.

D. EXTENSIBLE 3D (X3D)

Extensible 3D (X3D) "is an ISO-ratified, royalty-free open standards file format and run-time architecture to represent and communicate 3D scenes and objects" (What is X3D?, 2018). X3D is a type of markup language, evolving from older file formats such as Virtual Reality Markup Language (VRML). It is capable of integration with the backbone for common webpages, Hyper Text Markup Language (HTML) or dedicated engines such as InstantReality (What is X3D?, 2018).

X3D was evaluated as a possible output format for this thesis. Unity3D completes the radar detection envelope render as described in Chapter III, Section A and an X3D

exporter may be used to produce an X3D model of the radar volume, at correct 1:1 scale (Franke, 2017). This allows the model to be further manipulated or imported into an X3D graphical scene as shown in Figure 19. In addition, this allows for simplified sharing and archiving of the scenes in a compact format that does not require a license.

The exporter is publically available on the Github repository and was used as-is. It provides an additional menu option in the Unity developer interface that allows selected game objects to be exported to `.x3d` file format. The only adjustment made to the `.x3d` files for compatibility with the InstantReality X3D file viewer was to change the data sections corresponding to increase cell contrast and visibility.

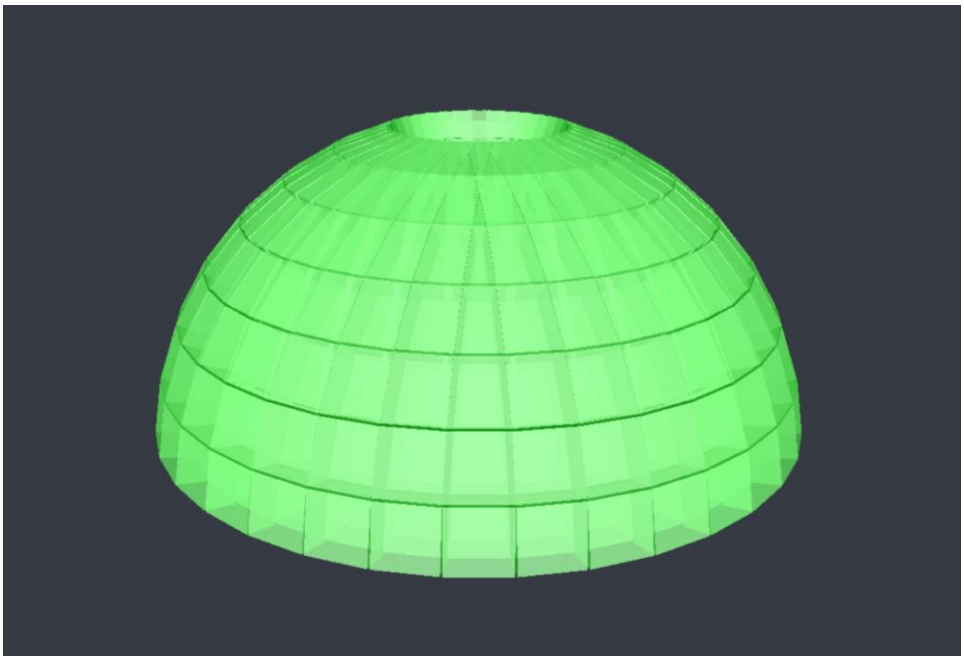

Figure 19. Radar Volume Depicted in X3D

IV. RADAR VISUALIZATION OUTPUTS

A. INTRODUCTION

The key objective of this project was to demonstrate three key phenomena that affect radar propagation, specifically atmospheric refraction, terrain masking, and multipath. This chapter contains screenshots from the development environment that are representative of the implementation of these phenomena. Section A describes two representative types of radars employed for each test case. Section B describes the observed variances in refraction caused by changes in meteorological conditions. Section C demonstrates the effects of terrain and multipath.

For quick recognition of scale in Unity, graphics are overlaid with a grid in the positive X, positive Y quadrant. The distance between each line represents 10 kilometers.

B. RADAR TYPES

To demonstrate the flexibility of the radar performance model, two different types of radar are represented. The specific parameters used to generate the volumes do not intentionally match any specific radars in production.

1. Air Surveillance Radar

Air Surveillance Radars (ASR) are designed to provide coarse target information at long ranges (generally in excess of fifty nautical miles). Many are only two-dimensional, providing the operator with target azimuth and range information only. They generally operate at lower frequencies and high power at low PRFs in order to increase unambiguous range at the cost of resolution. ASRs generally operate in the L band and below (Richards, Scheer, & Holm, 2010).

The representative radar was given an unambiguous range of 200km, a 5-degree beamwidth, and 1000m pulsewidth. Its envelope, absent refraction and terrain, is depicted in Figure 20. This program output matched expectations; without any atmospheric or terrain interactions, waves propagate away from the emitter in perfectly linear fashion.

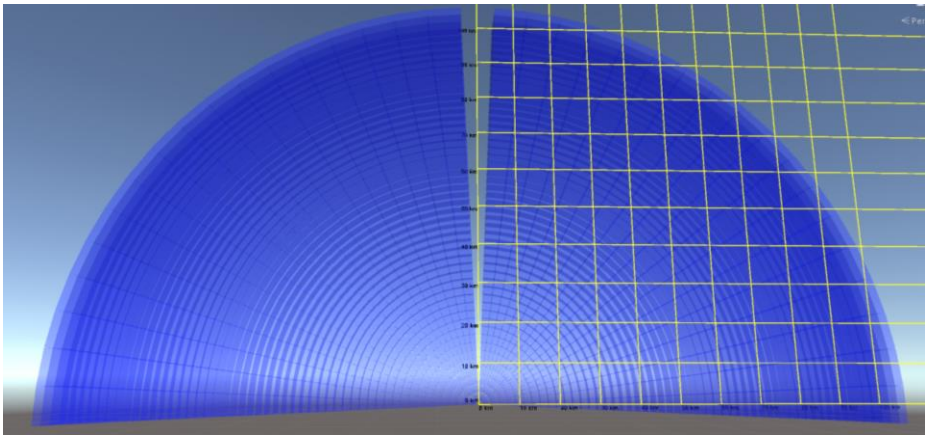

Figure 20. Air Surveillance Radar Volume (10km Grid Spacing)

2. Target Tracking Radar

Target Tracking Radars (TTR) are in many ways the opposite of ASRs. They are designed to provide very accurate range, speed, and altitude resolution, with sufficient granularity to guide a kill vehicle to the target at tactical ranges. This necessitates accuracy on the order of tens of meters, which can best be achieved with very high PRFs, generally in the X band or higher (Richards, Scheer, & Holm, 2010).

The representative radar was given an unambiguous range of 25km, a 1-degree beamwidth, and 500m pulsewidth. Its envelope, absent refraction and terrain, is depicted in Figure 21. As is the case in Figure 20, the output matches expectations.

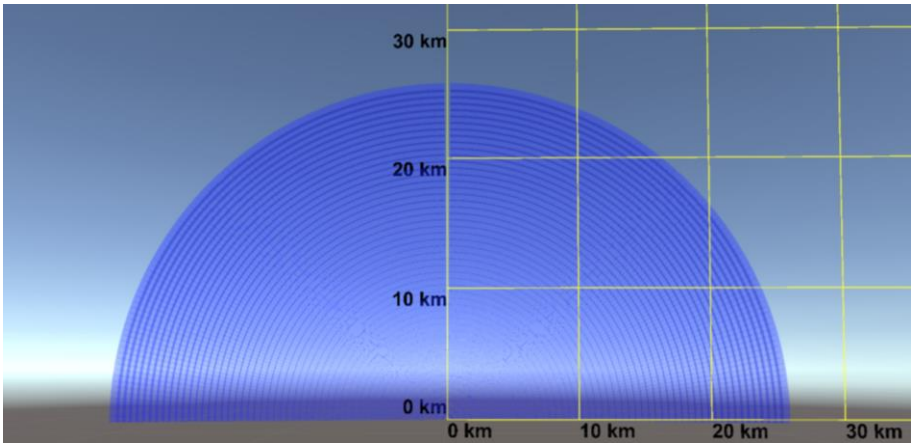

Figure 21. Target Tracking Radar Volume

C. OBSERVED REFRACTIVE EFFECTS

The refraction model used in this thesis is sensitive to three atmospheric parameters: pressure, temperature, and humidity. Figures 22 and 23 represent the program output for standard conditions, in which temperature and humidity are both highest at sea level and decrease as altitude increases. In Figure 24, the standard condition output is overlaid on the refraction-free output. Values for these meteorological arrays may be found in Appendix B, Table 2, and Appendix C, Table 3.

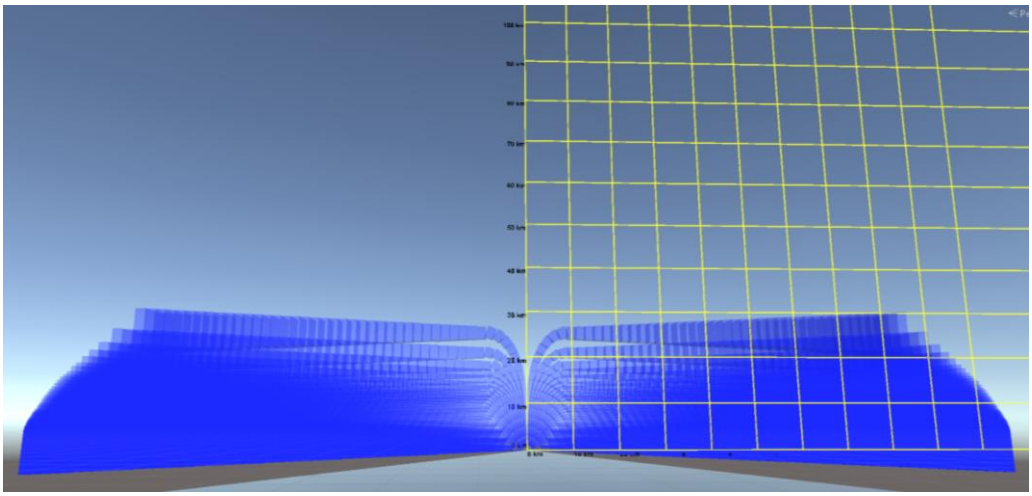

Figure 22. ASR Standard Atmospheric Refraction (10km Grid Spacing)

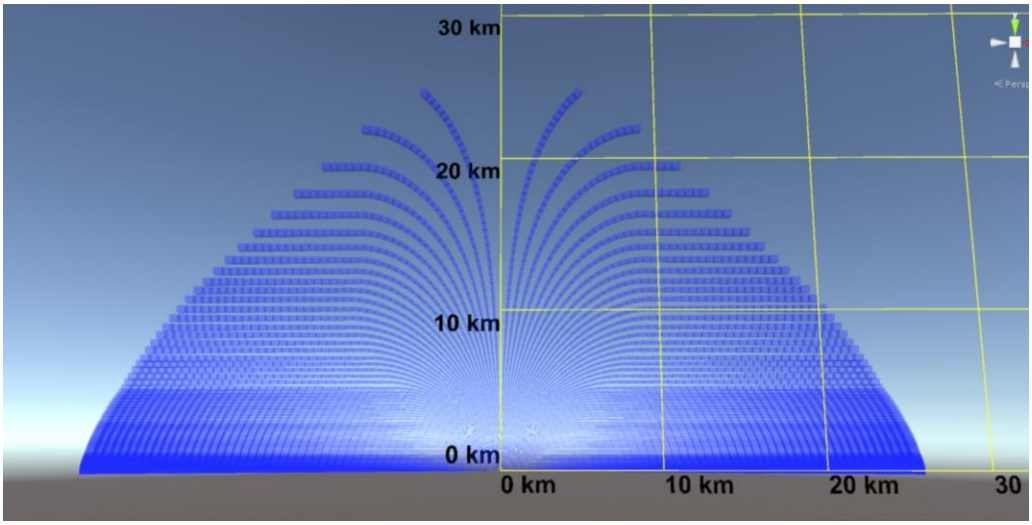

Figure 23. TTR, Standard Atmospheric Refraction

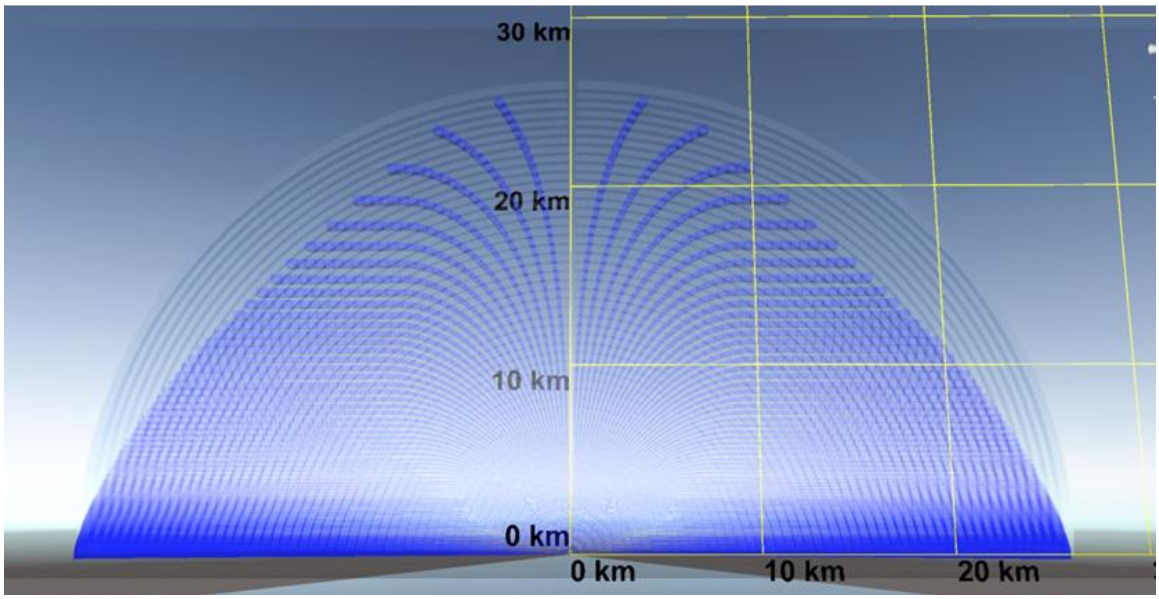

Figure 24. TTR Standard Refractive (Blue) on Non-Refractive (Grey)

The most notable effects of refraction include a flattening of the top of the envelope, as waves generally bend earthwards. At low altitudes, a similar phenomenon is observable. The denser, warmer, and more humid air all serve to increase refraction, and hence increase the bend in the waves. This leads to beams being compressed together in the lower altitudes, and bending these waves towards the Earth's surface. The increased density of coverage in the altitudes below ten kilometers is profound.

The model refractive effects generally appear similar to the distribution demonstrated in the background literature (Figure 5). Notably, the deviations from Figure 20 and 21 correspond well to the distribution representative of real-world radar performance described in Figure 6.

The project also included the ability to select alternative meteorological information. These alternatives represent non-standard weather, in which a temperature and/or humidity inversion occurs at two kilometers of altitude. Figures 25 and 26 represent the ASR and TTR propagation outputs for these alternative conditions. Figure 27 is the inversion model output over the standard refractive output. Values for the inversion meteorological arrays may be found in Appendix B, Table 2, and Appendix C, Table 4.

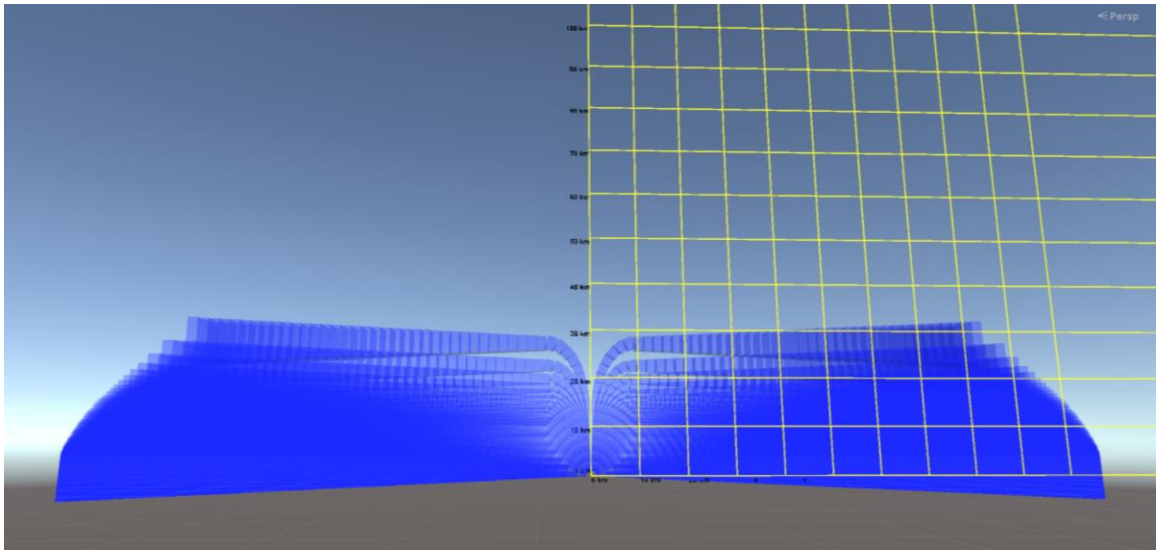

Figure 25. ASR Propagation (Humidity and Temperature Inversion, 10km Grid Spacing)

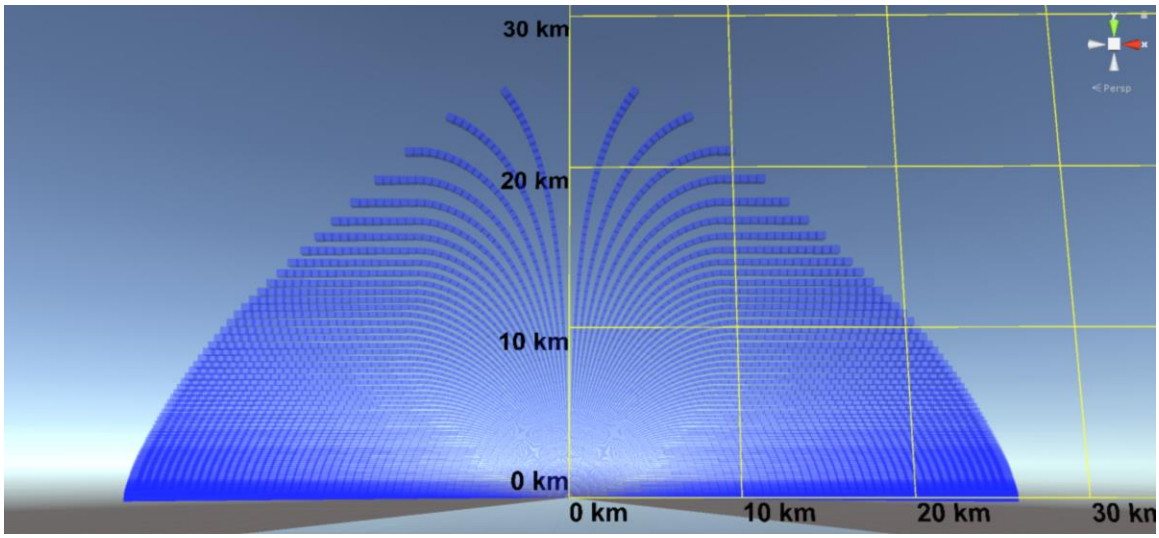

Figure 26. TTR Propagation (Humidity and Temperature Inversion)

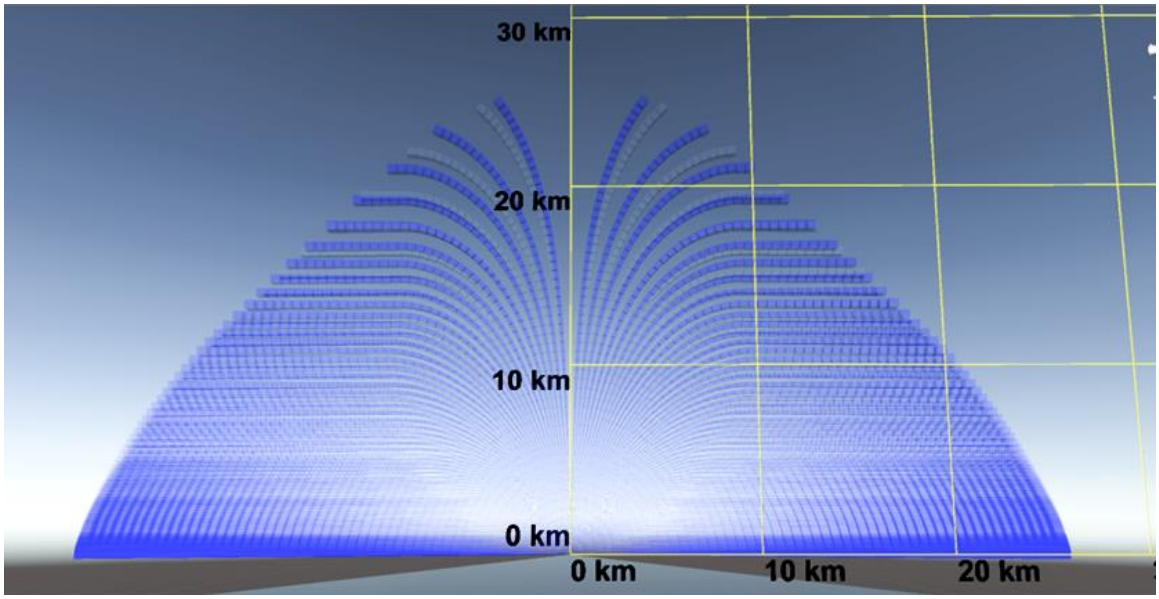

Figure 27. TTR Inversion Refractive (Blue) on Standard Refractive (Grey)

The comparison of the respective outputs demonstrates that waves experience less total refraction (defined by degrees from their start direction) in atmospheres in which a temperature and humidity inversion occurs. In other respects, the outputs are ultimately nearly identical.

This does not match expectations; based on background research in Chapter II, Section B, much more anomalous refraction was expected, especially at the altitudes that experienced the inversion in the model (between one and three kilometers).

An explanation for the similarity is the lack of lateral variance in the atmosphere model. Snell's Law would cause a wave in the model to experience no further changes to its path once both its altitude and atmospheric parameters cease to change. This means that once a wave's path has bent to near parallel with the Earth's surface, only a change in atmospheric parameters would cause any further deviation from its path – and in the US Standard Atmosphere model, there is no change in parameters to prompt this. This would explain the trend towards parallel observable in Figure 25 and 27.

D. TERRAIN MASKING AND MULTIPATH

Incorporating terrain was a key goal for the project. In order to accentuate its effects, the elevation data from the vicinity of Marine Corps Air Station (MCAS) Yuma was chosen due to the presence of significant terrain variance. Specifically, the emitter was placed at N32.30° W113.45°, represented in Figure 28, the color-coded heightmap generated by a MATLAB script (Tung, 2009).

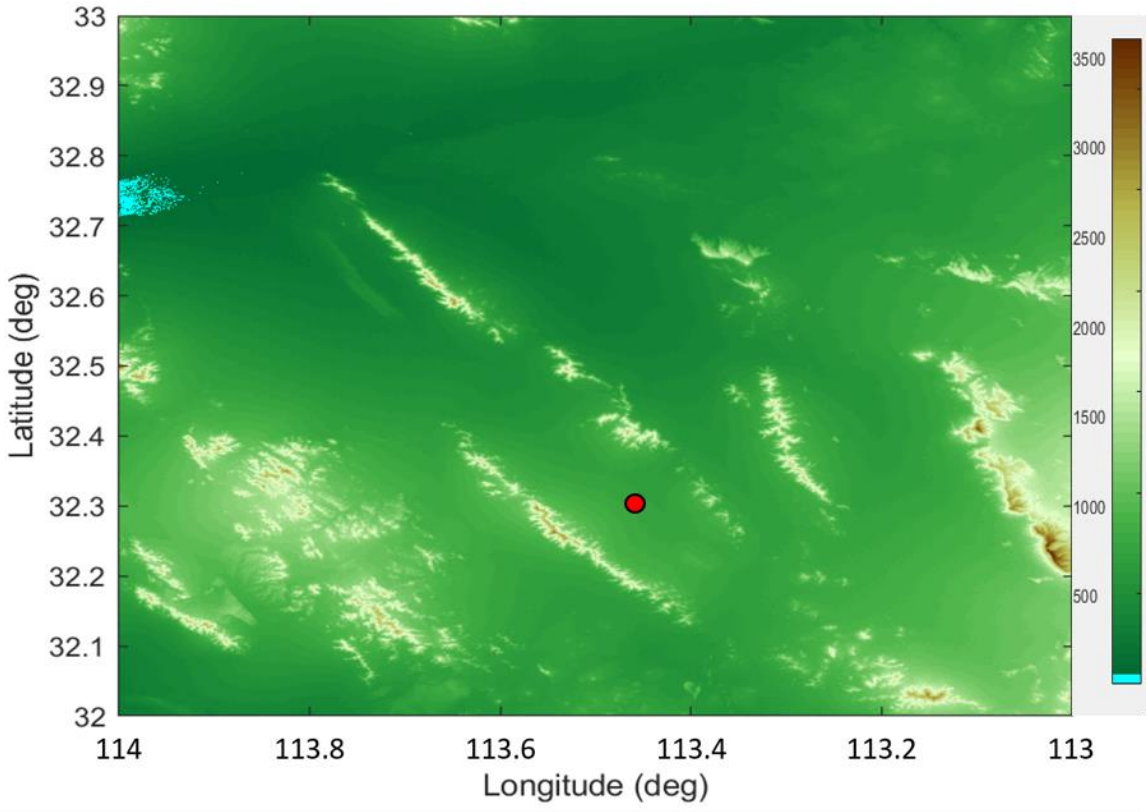

Figure 28. Heightmap from DTED for Geocoordinate N32 W113 (Altitude in Feet)

Per the descriptions in Chapter III, Section A, RRCs that are blocked by terrain are colored red, and no further cells are drawn. RRCs that pass within 0.6 beamwidths of terrain are colored yellow and the beam continues. This behavior is depicted in Figure 29 and 30 for ASRs and TTRs, respectively.

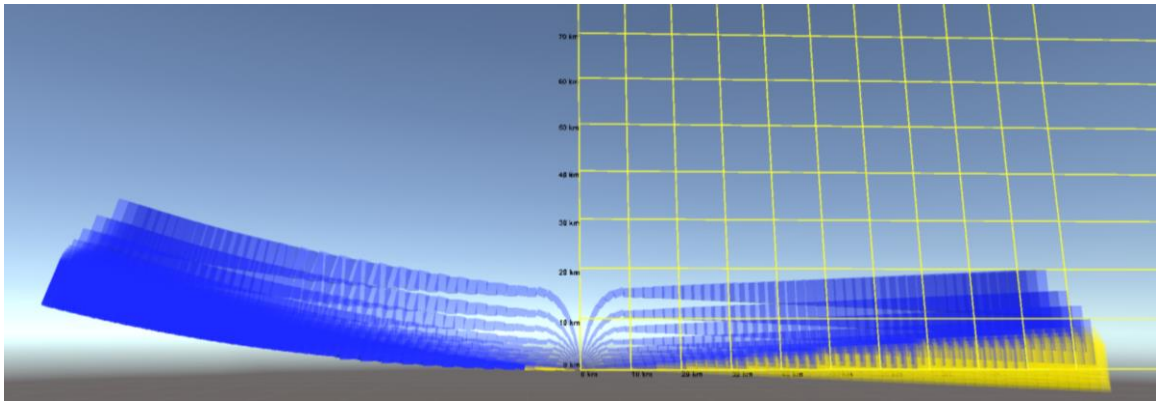

Figure 29. ASR Cross-Section with Terrain Masking, Standard Refraction (10km Grid Scale)

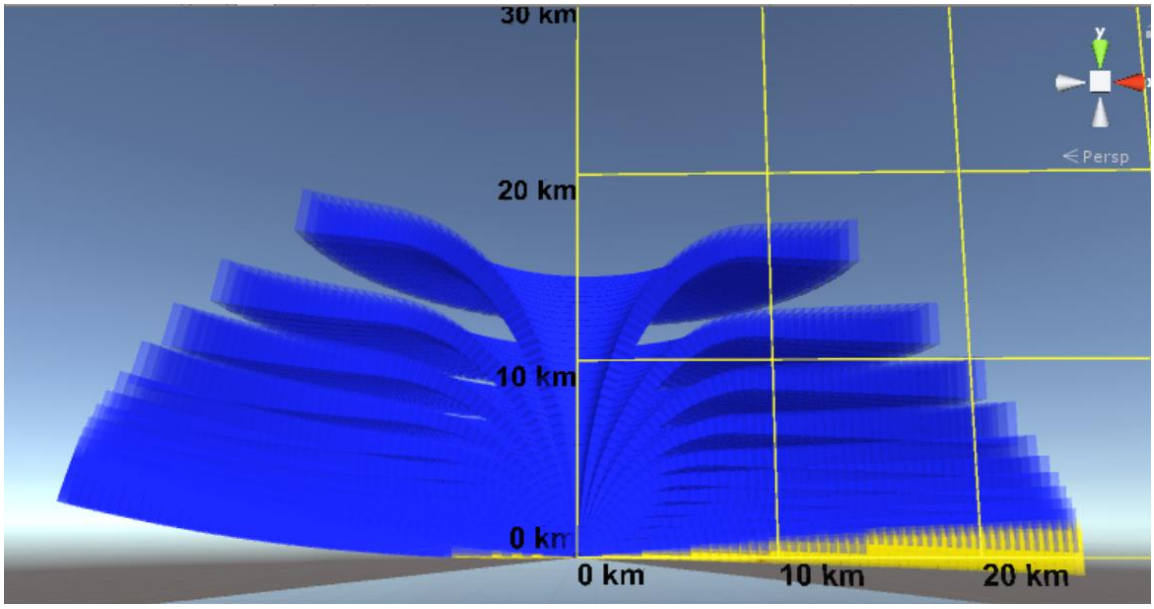

Figure 30. TTR Cross-Section with Terrain Masking, Standard Refraction

In addition to the vertical cross sections, the construction of the program allows the user to select specific output visualization options. Some of these include horizontal slices (Figure 31) which emphasizes the layer adjacent to terrain or at a specific altitude, or as an X3D scene output (Franke, 2017) that may be manipulated by the user, to include further export into fully realized Earth models or integration with other models in the X3D library (Figure 32).

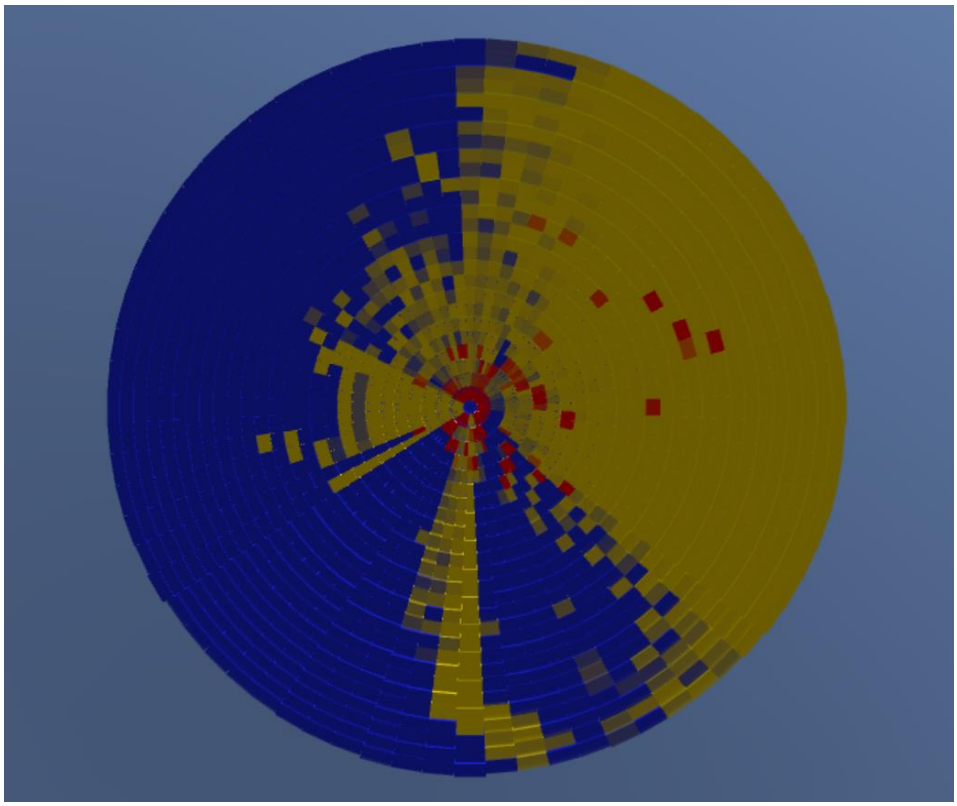

Figure 31. TTR Terrain Masking and Multipath (Bottom View)

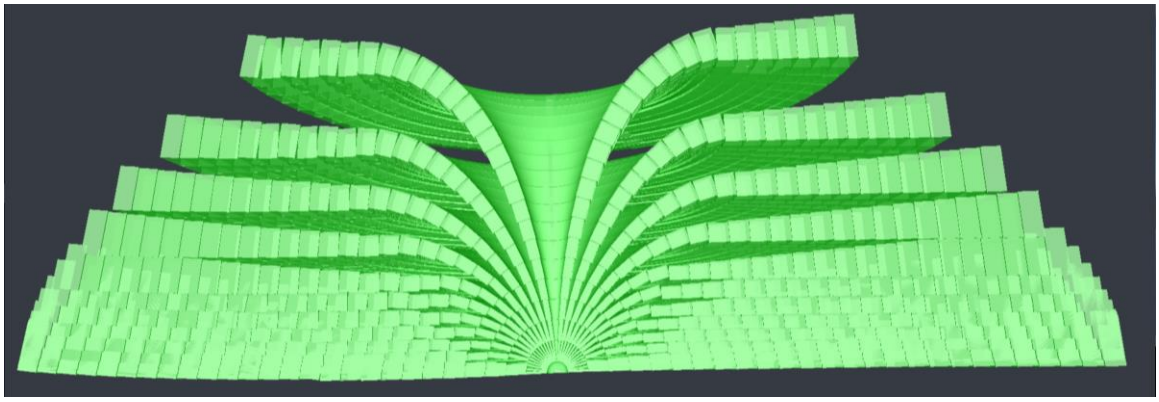

Figure 32. TTR Radar X3D Model

Integration with X3D Earth would allow the radar's propagation volume to be placed in the 3D terrain corresponding with its grid coordinate. This represents a significant increase in capability compared to current radar terrain masking methods, which generate outputs that look similar to Figure 31.

Terrain and multipath's influence on radar propagation met expectations. Even the relatively small mountains (~1000 meter variance from average terrain) in the sample DTED file resulted in significant multipath and terrain masking propagation impacts within 1-2 beamwidths of the horizon.

Propagation that was unaffected by masking or multipath directly demonstrated some deviation from expected refraction. This is likely due to how the atmospheric model was implemented (Chapter III, Section A). For the purpose of determining the parameters of the atmosphere, the height above terrain was used, vice height above zero MSL, resulting in a higher average altitude value, which returned lower humidity, temperature, and pressure. This results in decreased refraction compared to execution without terrain. The best means to correct this would be the inclusion of a fully featured atmospheric model, described in Chapter V, Section A.

The instructions to replicate these results may be found within Appendix D.

V. CONCLUSIONS AND FUTURE WORK

A. CONCLUSIONS

The implementation of the radar formulas using the Unity3D software package demonstrates that 3D volume representations of radar propagation are possible on consumer-grade hardware within reasonable computation time. The project also demonstrates that both atmospheric and terrain effects may feasibly be included in modeling radar performance and that these effects are significant enough to warrant inclusion.

However, the implementation does have a number of shortfalls. Due to this project's exploratory nature, computational efficiency was not a priority. Running the simulation with terrain takes in excess of thirty minutes to render when running on a low-end consumer-grade laptop without a graphics processing unit (GPU). This is likely caused by the size of the terrain data points array in memory and lack of dedicated optimizations, not an issue with the fundamental equations.

The use of the US Standard Atmosphere model was likely the greatest limitation on representing refraction. It vastly simplifies the behavior of the Earth's atmosphere and explains the absence of more anomalous propagation, including ducting. This makes the incorporation of fully featured meteorological data as described in Chapter V, Section A a priority for future work.

Despite the weaknesses in implementation, the comparison between the naïve model without refraction or terrain (Figures 20 and 21) and the models that include the refraction described in Chapter III, Section A, demonstrate the considerable differences between propagation caused by the atmosphere. Neglecting to include these effects vastly misrepresent a radar's capabilities, and the implementation of these effects in simulation must be a capability included within future mission planning tools.

B. FUTURE WORK

There are significant opportunities to increase the value of the program for mission planners. The implementation of more accurate and/or location-specific parameters would be the most accessible next step. The inclusion of a more detailed weather model would then be the next logical improvement. Finally, the addition of additional capabilities, notably probability-of-detection modeling and automatic pathfinding would be the ultimate step.

1. Live Validation

While the results presented in Chapter IV generally match expectations developed by the research in Chapter II, the only way to truly demonstrate the validity of the model is to test real radars in quantified meteorological conditions.

Prescribing the specifics of the testing protocol is well outside the scope of this project, but validating the refraction profile and shadow zone graphs in Chapter IV would be incredibly valuable in building warfighter trust in radar performance models. No matter how robust the math, operators are unlikely to trust it until it has been proven in live conditions. Data collected from real-world experimentation would also be valuable in refining the models and validating assumptions.

2. METOC Integration

One of the most significant limitations of this thesis is the assumption that the atmosphere is constant at every latitude and longitude for all equivalent altitudes. Within this model, there is no lateral change in atmospheric parameters at the same altitude e.g. the pressure, temperature, and humidity at ten kilometers above geocoordinate N30, W110 are identical to the pressure, temperature, and humidity ten kilometers above geocoordinate N90, W90 (Ribando, 2018). This does not represent specific tactical conditions.

As described in Chapter IV, Section B, the observed variance between atmosphere models was lower than expected, and refractive phenomenon were minimized by its simplicity. The similarities in refraction across atmospheres would be corrected by including a more fully featured atmosphere model.

Additionally, the ability to use live data collected from sensors in the field would greatly increase the fidelity of the model and provide a new capability to mission planners, who have heretofore employed generic models and simple 2D cross sections. To this end, integrating this project with meteorological databases must be a priority for future work.

3. Increased Parameterization

This project has described emitters in the most general terms possible, considering only beamwidth, pulse width, and range. Adding in the ability to describe more complicated features, such as effective radiated power, antenna aperture size, efficiencies, operating frequency, and other parameters would allow for the next level of evaluation – the ability to define the intensity, or power per unit area, within each RRC.

This would add significantly more value than the simple color-coding present in its current version, and lead into additional capabilities, including calculating probability of detection, or applying the model to noise jammers or communications. Adapting the model to also represent airborne radars would also be invaluable.

4. Data Visualization

The volumetric depiction is just the most basic of visualization means. With further development, the system could automatically produce shadow zone graphs, depicting the amount of shadowed airspace available for unobserved flying, or provide the option to flatten the Earth's surface, presenting terrain in a more human-readable way.

Automating the process of slicing the volume would also be useful for speeding up the mission planning process, allowing planners to generate the required graphics quickly and efficiently. Providing the user with an intuitive and powerful interface would be essential for future iterations of this project.

5. Probability-of-Detection Simulation

Modeling probability-of-detection (P_d) is the ultimate goal of any radar visualization project. Successfully representing this further reduces the uncertainty of radar performance, giving mission planners the ability to quantify what risks they are willing to

assume, and ultimately choose the least risk, highest reward flight paths. Adding this capability is a natural extension of any radar visualization project.

It is important to note that this project's propagation model is both frequency and power agnostic. It does not account for the varying amounts of absorption that different frequencies experience or capture the path of energy returning from a target to the emitter. However, based on the distance and time-of-travel, calculating the intensity within any given RRC would be a trivial addition, and, coupled with the already quantified angle of incidence, the essential inputs to the radar range equation would be in place (Cheng, 2016).

6. Pathfinding

The next natural opportunity the project presents is the ability to generate unobserved paths through the volume. Through the use of A* or other search algorithms, it would be possible to automatically generate flight paths that would either allow aircraft to close to unobserved weapons release points or to pass through undetected.

Especially when coupled with more definite probability of detection models and specific emitter parameters, the opportunities presented by pathfinding provide the means to greatly increase the speed and efficacy of mission planning.

7. Incorporation into Battlefield Simulation

Because radars employed in a military context are often associated with a variety of weapon systems, supporting forces, and other similar and dissimilar radars, incorporating this model into a greater military simulation, or at the very least, allowing for multiple radars to be represented would increase the applicability of this project, both to simulations and real-world operations.

APPENDIX A. FREQUENCY BANDS

Table 1. Frequency Bands. Adapted from Barton (2005).

Band Designation	Nominal Frequency Range
HF	3 - 30 MHz
VHF	30 - 300 MHz
UHF	300 - 1,000 MHz
L	1,000 - 2,000 MHz
S	2,000 - 4000 MHz
C	4,000 - 8000 MHz
X	8,000 - 12,000 MHz
K_u	12 - 18 GHz
K	18 - 27 GHz
K_a	27 - 40 GHz
V	40 - 75 GHz
W	75 - 110 GHz
Mm	110 - 300 GHz

THIS PAGE INTENTIONALLY LEFT BLANK

APPENDIX B. TEMPERATURE AND PRESSURE MODELS

Table 2. U.S. Standard Atmosphere. Adapted from Ribando (2015).

Alt. (km)	Temp. (K)	Pressure (Pa)	Density (kg/m^3)
0	288.15*	101.33	1.225
1	281.651*	89.88069	1.11166
2	275.1541*	79.50535	1.006554
3	268.6592	70.1246	0.909254
4	262.1663	61.66346	0.819347
5	255.6755	54.0509	0.736428
6	249.1867	47.21991	0.660111
7	242.7	41.10722	0.590018
8	236.2152	35.65328	0.525785
9	229.7325	30.8021	0.467062
10	223.2519	26.50108	0.413509
11	216.7733	22.70095	0.3648
12	216.65	19.40027	0.311936
13	216.65	16.58031	0.266594
14	216.65	14.17095	0.227854
15	216.65	12.11229	0.194753
16	216.65	10.35322	0.166469
17	216.65	8.850047	0.1423
18	216.65	7.565491	0.121645
19	216.65	6.467703	0.103994
20	216.65	5.529479	0.088908
21	217.581	4.729078	0.075713
22	218.5743	4.047606	0.064508
23	219.5672	3.466954	0.055004
24	220.5599	2.971816	0.046937
25	221.5522	2.549275	0.040083
26	222.5443	2.188419	0.034256
27	223.536	1.880007	0.029297
28	224.5274	1.61622	0.025075
29	225.5186	1.390436	0.021478
30	226.5093	1.197043	0.018409
31	227.4998	1.031268	0.015791
32	228.49	0.889067	0.013555
33	230.9737	0.767311	0.011572
34	233.7445	0.663412	0.009887
35	236.5144	0.574593	0.008463
36	239.2834	0.49852	0.007257
37	242.0516	0.433245	0.006235
38	244.8189	0.377135	0.005366

39	247.5854	0.328817	0.004626
40	250.351	0.287139	0.003995
41	253.1157	0.251128	0.003456
42	255.8796	0.219963	0.002995
43	258.6426	0.192947	0.002599
44	261.4047	0.169492	0.002259
45	264.166	0.149097	0.001966
46	266.9264	0.131337	0.001714
47	269.686	0.115847	0.001496
48	270.65	0.102292	0.001317
49	270.65	0.090333	0.001163
50	270.65	0.079776	0.001027
51	270.65	0.070455	0.000907
52	269.0291	0.062212	0.000806
53	266.2747	0.054871	0.000718
54	263.5212	0.048335	0.000639
55	260.7685	0.042522	0.000568
56	258.0167	0.037359	0.000504
57	255.2657	0.032779	0.000447
58	252.5156	0.028721	0.000396
59	249.7663	0.02513	0.00035
60	247.0179	0.021957	0.00031
61	244.2703	0.019156	0.000273
62	241.5236	0.016687	0.000241
63	238.7778	0.014514	0.000212
64	236.0328	0.012604	0.000186
65	233.2887	0.010928	0.000163
66	230.5454	0.00946	0.000143
67	227.8029	0.008174	0.000125
68	225.0614	0.007052	0.000109
69	222.3206	0.006073	9.52E-05
70	219.5807	0.00522	8.28E-05

* 0, 1, and 2 km blocks are replaced with the following values for inversion: 283.15, 295.65, and 278.15, respectively. All others are unchanged.

APPENDIX C. HUMIDITY

Table 3. Representative Standard Day (Wet Climate) Adapted from Palchetti, Bianchini, Carli, Cortesi, and Del Bianco (2008).

Altitude (km)	Partial Pressure of H_20 (hPa)
0	23.371000000
1	12.780000000
2	9.123900000
3	5.467800000
4	3.090300000
5	0.712800000
6	0.418665000
7	0.124530000
8	0.076215000
9	0.027900000
10	0.024619000
11	0.021338000
12	0.011617500
13	0.001897000
14	0.001490750
15	0.001084500
16	0.000678250
17	0.000272000
18	0.000226259
19	0.000113600
20	0.000057036
21	0.000028636
22	0.000014378
23	0.000007219
24	0.000003624
25	0.000001820
26	0.000000914
27	0.000000459
28	0.000000230
29	0.000000116
30	0.000000058
31	0.000000029
32	0.000000015
33	0.000000007

Table 4. Representative Low Altitude Humidity Inversion Model (Dry Climate). Adapted from Palmisano (2014).

Altitude (km)	Partial Pressure of H_20 (hPa)
0	5.8
1	6.2
2	3.1
3	1.04
4	0.25
5	0.05
6	0.05
7	0.05
8	0.05
9	0.05
…*	…

*Values for 10km and above become insignificant. Standard model was used.

APPENDIX D. IMPLEMENTATION AND CODE REPOSITORY

This appendix assumes basic familiarity with Unity3D and MATLAB. It contains the instructions for accessing the code used to implement the Radar Envelope Visualization project. The files are all available on the Naval Postgraduate School Gitlab repository under the project name "RadarEnvelopeVisualization," at URL:

https://gitlab.nps.edu/datan/RadarEnvelopeVisualization

A. PROJECT STRUCTURE

The project-specific files are all contained within the project's Assets folder. This folder contains the Unity scene file that implements the visualization, the X3D output script, and four subfolders with specific dependencies. The contents of the project folder are depicted in Figure 33.

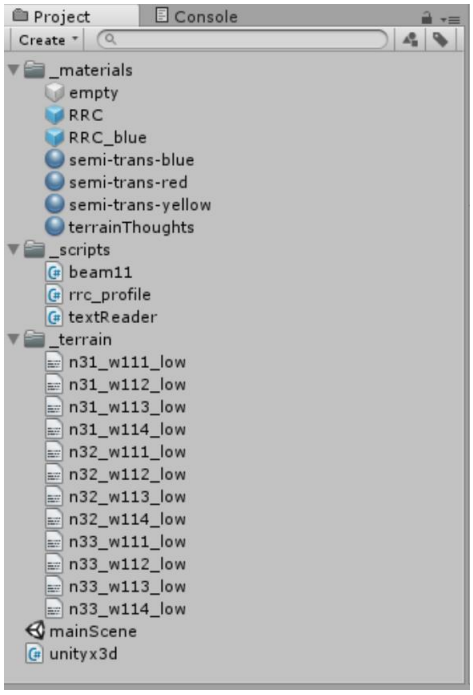

Figure 33. Project Contents In Unity Editor

The file `mainScene` contains the mapping between scripts, text files containing DTED data, materials, and prefabs. It also includes a legend and a number of cameras allowing for preselected radar volume viewpoints. The full scene hierarchy is represented in Figure 34.

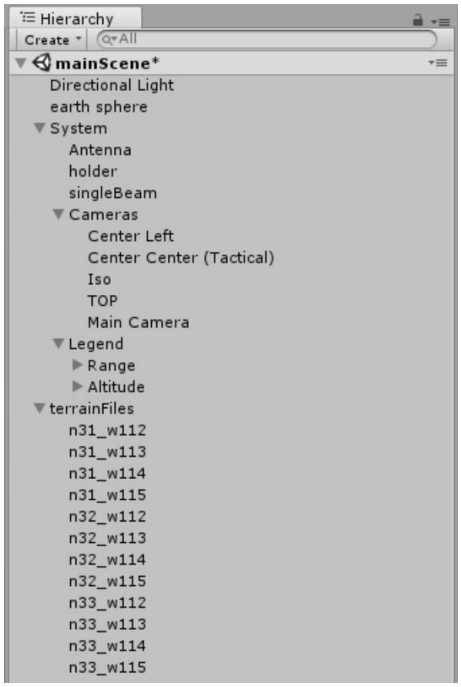

Figure 34. Scene Hierarchy

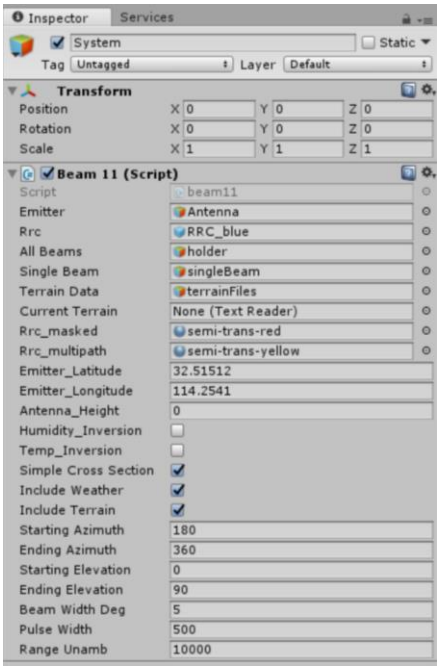

Figure 35. Inspector View of System Object

Within the System inspector view, the user-selected options include the emitter location parameters, a series of checkboxes, altitude and azimuth coverage options, and radar parametrics. Full documentation for these options is available on the NPS Gitlab repository.

B. UNITY SCENE SETUP

The `textReader` script that parses each individual DTED text file must run before the main script. To accomplish this, within the Unity editor, select the "Script Execution Order" option from within the Edit, Project Settings menu. Within the inspector, ensure that `textReader` has a lower default time than the main script. This selection is depicted in Figure 36.

Once that has been completed, ensure the parameters depicted in Figure 35 are filled in to the user's satisfaction, and click the play button within the Unity editor. Note that increasing azimuth and elevation coverage, decreasing pulse width or beamwidth, and increasing range will all dramatically increase the time needed to perform a render.

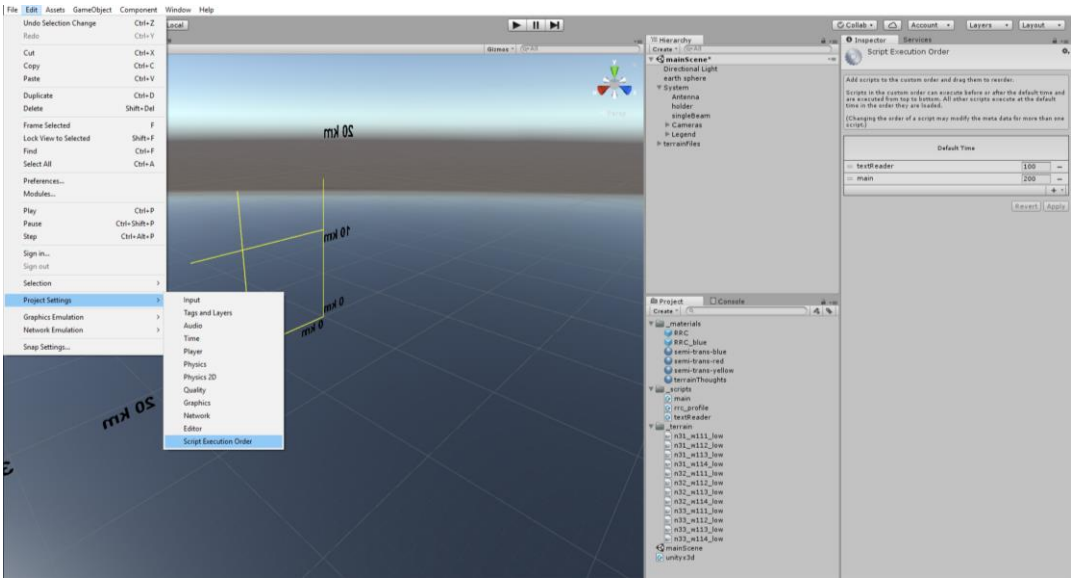

Figure 36. Script Execution Order

C. DTED ACQUISITION AND PREPARATION

DTED files may be acquired from any source; however, they must be in the correct `.dt2` hexadecimal format. Once the desired area has been downloaded, they must be converted into text files for the project to read. This is accomplished via a MATLAB script acquired from the MathWorks repository (Tung, 2009), located at URL:

https://www.mathworks.com/matlabcentral/fileexchange/25897-read-dted-elevation-data

The project's Gitlab repository includes sample converted DTED files for the vicinity of MCAS Yuma. They have been downsampled to 500 by 500 elevation posts in order to reduce memory costs. In the Unity scene, each of these converted DTED files is then associated with an empty game object and placed within the scene hierarchy in the "terrainFiles" folder for reference.

D. X3D EXPORT

Once the radar propagation volume has been generated, the RRCs may be exported as an X3D scene. To accomplish this, a Unity3D to X3D converter was acquired from a Github repository (Franke, 2017), located at URL:

https://github.com/thefranke/unityx3d

Once the single `.cs` script file from the repository is placed in the Assets folder, the export option will become available from the Unity3D scene view, within the Assets menu tab.

To export, first select all the game objects that are to be included within the X3D scene. The user then enters the Assets menu, and selects “Export X3D…” from within the X3D subheading (as depicted in Figure 37). After the user enters a name for the new X3D scene, Unity3D will produce a progress bar and the export will take place, yielding a similar result to Figures 19 and 32, except that the cells will all default to a white color.

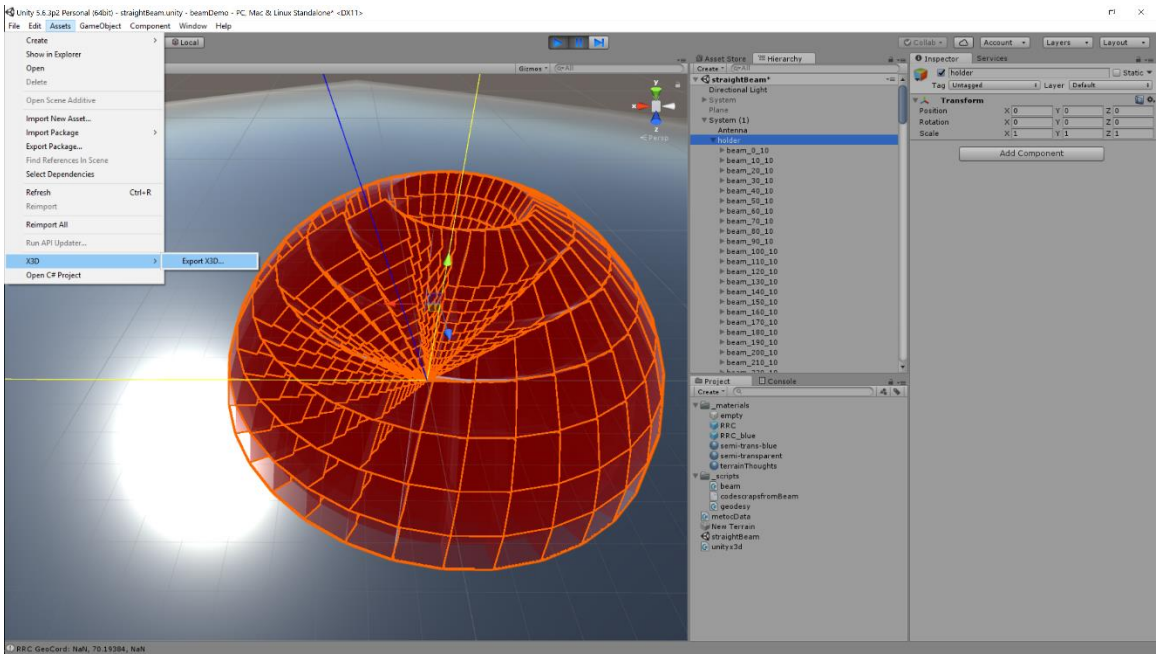

Figure 37. Using the X3D Exporter

THIS PAGE INTENTIONALLY LEFT BLANK

LIST OF REFERENCES

Air Combat Command Public Affairs Office. (2014, April 11). *F-35A Lightning II.* Retrieved November 17, 2017, from U.S. Air Force: http://www.af.mil/About-Us/Fact-Sheets/Display/Article/478441/f-35a-lightning-ii-conventional-takeoff-and-landing-variant/

Avionics Department. (2013). *Electronic warfare and radar systems engineering handbook.* Point Mugu, CA: Naval Air Warfare Center Weapons Division.

Barton, D. K. (2005). *Radar system analysis and modeling.* Norwood, MA: Artech House.

Bell, S. (2012). *A beginner's guide to humidity measurement.* Retrieved from National Physical Laborator 2: http://www.npl.co.uk/upload/pdf/Beginner%27s%20guide%20to%20humidity%20measurement%20(draft%20for%20comment).pdf

Ben Cheikh, T. L., & Guillemette, P. (2017). GPU ray tracing-based method for real-time ISAR simulation. Paper presented at Interservice/Industry Training, Simulation, and Education Conference, Orlando, FL.

Cheng, Y.-P. (2016). *Hybrid high-fidelity modeling of radar scenarios using atemporal, discrete-event and time-step simulation* (Master's thesis). Retrieved from https://calhoun.nps.edu/handle/10945/51670

Department of Defense. (1997). *Global climatic data for developing military products* (MIL-HDBK-310). Washington, DC: Department of Defense. Retrieved from http://everyspec.com/MIL-HDBK/MIL-HDBK-0300-0499/download.php?spec=MIL_HDBK_310.1851.pdf

Durland, N. H. (2009). Defining mean sea level in military simulations with DTED. *Proceedings of the 2009 Spring Simulation Multiconference* (p. 115). Society for Computer Simulation International. Retrieved from https://dl.acm.org/citation.cfm?id=1639931

Franke, T. A. (2017, August 9). A script to import/export X3D to/from Unity. Retrieved from Github: https://github.com/thefranke/unityx3d

Koler, O., & Shintel, T. (2017). Enhanced aerial radar line of sight performance. Paper presented at Interservice/Industry Training, Simulation, and Education Conference, Orlando, FL.

Leary, J. J. (1995). *Search for a stealthy flight path through a hostile radar defense network* (Master's thesis). Retrieved from https://calhoun.nps.edu/bitstream/handle/10945/31582/95Mar_Leary.pdf.

Mangum, J. G., & Wallace, P. (2015, March 30). Atmospheric refractive electromagnetic wave bending and propagation delay. *Publications of the Astronomical Society of the Pacific 127*(947), 74.

NIMA. (2000). *Performance specification digital terrain elevation data (DTED),* (MIL-PRF-89020B). Springfield, VA: NIMA. Retrieved from https://dds.cr.usgs.gov/srtm/version2_1/Documentation/MIL-PDF-89020B.pdf

Palchetti, L., Bianchini, B., Carli, U., Cortesi, & Del Bianco, S. (2008). Measurement of the water vapour vertical profile and of the Earth's outgoing far infrared flux. *Atmospheric Chemistry and Physics, 8*(11), 2885-2894. Retrieved from https://www.atmos-chem-phys.net/8/2885/2008/acp-8-2885-2008.pdf

Palmisano, J. (2014). *High altitude balloon tutorial - measuring humidity*. Retrieved from http://www.societyofrobots.com/space_balloon_humidity_test.shtml

Plait, P. (2009, January 15). How far away is the horizon? [Blog post]. Retrieved from http://blogs.discovermagazine.com/badastronomy/2009/01/15/how-far-away-is-the-horizon/#.WuIlGcgvwb1

Ribando, R. J. (2018, March 20). *Free excel\VBA spreadsheets for heat transfer*. Retrieved from UVA Faculty Webserver: http://www.faculty.virginia.edu/ribando/modules/xls/

Richards, M. A., Scheer, J. A., & Holm, W. A. (2010). *Principles of modern radar vol. I: basic principles.* Raleigh: SciTech Publishing, Inc.

Sandwell, D.T. (2002). *Reference Earth Model – WGS84*. Retrieved from UCSD Webserver: http://topex.ucsd.edu/geodynamics/14gravity1_2.pdf

Stone, J. A., & Zimmerman, J. H. (2011, December 28). *Refractive index of air calculator*. Retrieved from Engineering Metrology Toolbox: https://emtoolbox.nist.gov/wavelength/documentation.asp

Tung. (2009, Nov 9). Retrieved from Mathworks: https://www.mathworks.com/matlabcentral/fileexchange/25897-read-dted-elevation-data

What is X3D? (2018, May 9). Retrieved from web3D: http://www.web3d.org/x3d/what-x3d/

Williams, L. (1978). Casting curved shadows on curved surfaces. *ACM Siggraph Computer Graphics (Vol. 12, No. 3)*, 270-274.

Wolff, C. (n.d.). *The resolution cell*. Retrieved from Radar Tutorial: http://www.radartutorial.eu/01.basics/The%20resolution%20cell.en.html

THIS PAGE INTENTIONALLY LEFT BLANK

INITIAL DISTRIBUTION LIST

1. Defense Technical Information Center
   Ft. Belvoir, Virginia

2. Dudley Knox Library
   Naval Postgraduate School
   Monterey, California